Physics – Uspekhi **66** (12) 1262 – 1276 (2023)

METHODOLOGICAL NOTES PACS numbers: 95.30.Qd, 97.10.Gz

Magnetorotational instability in Keplerian disks: a nonlocal approach

N I Shakura, K A Postnov, D A Kolesnikov, G V Lipunova

DOI: https://doi.org/10.3367/UFNe.2023.09.039554

Contents

Abstract. We revisit the modal analysis of small perturbations in Keplerian ideal gas flows with a constant vertical magnetic field leading to magnetorotational instability (MRI) using the nonlocal approach. In the general case, MRI modes are described by a Schrödinger-like differential equation with some effective potential, including 'repulsive' $(1/r^2)$ and 'attractive' $(-1/r^3)$ terms, and are quantized. In shallow potentials, there are no stationary 'energy levels.' In thin Keplerian accretion discs, the perturbation wavelengths $\lambda = 2\pi/k_z$ are smaller than the disc semi-thickness h only in 'deep' potential wells. We find that there is a critical magnetic field for the MRI to develop. The instability arises for magnetic fields below this critical value. In thin accretion discs, at low background Alfvén velocity $c_{\rm A} \ll (c_{\rm A})_{\rm cr}$, the MRI instability increment ω is suppressed compared to the value obtained in the local perturbation analysis, $\omega \approx -\sqrt{3}{\rm i}c_{\rm A}k_z$. We also investigate for the first time the case of a radially variable background magnetic field.

Keywords: magnetorotational instability, accretion discs

N I Shakura [1,a], **K A Postnov** [1,2,b], **D A Kolesnikov** [1,3,c], **G V Lipunova** [1,4,d]
[1] Lomonosov Moscow State University, Sternberg State Astronomical Institute, Universitetskii prosp. 13, 119234 Moscow, Russian Federation
[2] Kazan Federal University, ul. Kremlevskaya 18, 420111 Kazan, Russian Federation
[3] The Raymond and Beverly Sackler School of Physics and Astronomy, Tel Aviv University, Tel Aviv 69978, Israel
[4] Max-Planck-Institut für Radioastronomie, Auf dem Hügel 69, 53121 Bonn, Germany
E-mail: [a] nikolai.shakura@gmail.com, [b] kpostnov@gmail.com, [c] kolesnikovkda@gmail.com, [d] galja@sai.msu.ru

Received 16 December 2022, revised 21 September 2023
Uspekhi Fizicheskikh Nauk **193** (12) 1340 – 1355 (2023)
Translated by the authors

1. Introduction

Shear flows in astrophysical objects, characterized by an inhomogeneous velocity field, are a universal source and agent of energy transport and are closely related to the phenomena of turbulence [1–3], magnetic field generation [4], and particle acceleration [5].

The stability of shear hydrodynamic flows with respect to small perturbations in a magnetic field in laboratory conditions was first considered in papers by E Velikhov [6] and S Chandrasekhar [7]. In the absence of a magnetic field, hydrodynamic instability in a rotating shear flow appears when the angular momentum decreases outward from the axis of rotation [8].

Velikhov and Chandrasekhar showed that, in a vertically magnetized, axisymmetric, differentially rotating flow with angular velocity decreasing outward, magnetorotational instability (MRI) is possible.[1]

The theory of MRI was applied to astrophysical accretion disks in an influential paper by [10], and it is now believed that this instability generates turbulence in accretion disks (see review [11]). Nonlinear numerical simulations (e.g., [12–14]) confirm that MRI can indeed sustain turbulence in accretion disks.

It is believed that, for the study of MRI and analysis of its properties, a local approximation in an ideal incompressible fluid is sufficient, where small perturbations are taken in cylindrical coordinates r, z, ϕ in the form of plane waves $\sim \exp[{\rm i}(\omega t - k_r r - k_z z)]$. In this case, the differential MHD equations are transformed into algebraic equations, the dispersion relation for perturbations is found in the form of a biquadratic equation [10, 15], and the instability increment does not depend on the magnetic field (see Eqns (77) and (78)

[1] We consider only the case of a vertical background magnetic field. Axisymmetric gas flows with toroidal background magnetic fields in the presence of gravity are subject to Parker instability [9].

below, respectively). Taking into account nonideal effects in this approximation slightly changes the conditions for the occurrence of MRI but leaves qualitatively the same picture [16, 17].

However, already in the pioneering work by Velikhov [6], a global analysis of long-wave disturbances in the direction perpendicular to the plane of the main flow was carried out for flows between two rotating conducting cylinders with a constant angular momentum over the radius, $\Omega(r)r^2 = \text{const}$. Radial perturbations were found from the solution to the Sturm–Liouville boundary value problem (in the Wentzel–Kramers–Brillouin (WKB) approximation). It was shown that such an approach implies a critical magnetic field, above which instability is suppressed, and the dependence on the boundary conditions remains even when the outer cylinder is extended to infinity.

Due to the potential importance of MRI in the emergence of turbulence in disk flows (accretion and protoplanetary disks, gaseous disks in galaxies), extensive analytical and numerical investigations of MRI were conducted in the 1990s–2000s in the approximation of incompressible fluid in a homogeneous magnetic field, including a global analysis of this instability. Nonlocal analysis shows that, in shear flows, the dispersion equation for the mode $\omega(k)$ contains a term dependent on radius as ($\propto -1/r^2$), which is usually neglected in local modal analysis. As expected, a critical value of the magnetic field appears in the global analysis, above which MRIs are stabilized [18–22]. For accretion disks around a central gravitational body, the obtained results depend on the choice of boundary conditions for perturbations at the inner and outer radii of the flow [22–24]. The choice of boundary conditions affects the discretization of local dispersion relations [22].

Despite the considerable previous scrutiny of this problem, in this study, we independently and comprehensively perform a nonlocal linear analysis of MRI in Keplerian accretion disks with angular velocity $\Omega(r) \propto 1/r^{3/2}$. We derive a dispersion equation that can be reduced to a Schrödinger-like equation with an 'energy' $E = -k_z^2$ and an effective potential $U(r)$ consisting of two terms: an 'attractive' term proportional to $\propto -1/r^3$ and a 'repulsive' term proportional to $\propto 1/r^2$. In contrast to the local analysis, the effective potential vanishes at a point r_0, which depends on the mode frequency ω, the wave number k_z, and the background Alfvén velocity. We examine in detail both cases where the outer radius of the disk, r_{out}, is greater or less than r_0. We numerically solve the boundary value problem for radial boundary conditions corresponding to both rigid and free flow boundaries. We emphasize the significance of the position of the flow boundaries relative to the zero points of the effective potential, appearing in the nonlocal analysis for the Sturm–Liouville boundary problem.We demonstrate that, in 'shallow' effective potentials, there can be a situation, depending on the position of the inner flow boundary, where MRIs do not occur. Such a situation is possible for flows around normal stars with large radii. Naturally, for flows around compact objects, the potential wells are very deep, and the energy spectrum is nearly continuous. We explicitly derive the critical magnetic field value that suppresses MRI and find the dependence of the MRI increment on the background homogeneous magnetic field. We consider for the first time the case of a background magnetic field that varies with radius in a power-law manner. We also examine the case of an incompressible fluid with density depending on the radial coordinate, where the equations for small perturbations remain the same as for a constant density, while the effective potential changes.

The structure of the paper is as follows. In Section 2, we perform a linear modal analysis for small perturbations in an ideal fluid in the form $\propto f(r)\exp[\mathrm{i}(\omega t - k_z z)]$. In Section 2.5, we derive the algebraic dispersion equation $\omega(k_z)$ and the critical Alfvén velocity below which MRI occurs. In Section 3.2, we consider for the first time MRI in the presence of a radially varying vertical magnetic field and demonstrate that, in this case, the effective potential can change nontrivially. In Section 4, we compare our results with the standard results obtained in the local modal analysis. In Appendix A, we numerically solve the Schrödinger equation for nonlocal perturbations with a constant background Alfvén velocity when the external radius of the flow, r_{out}, is greater than the zero radius of the effective potential r_0. In Appendix B, we consider the case of $r_{\text{out}} < r_0$, when the problem reduces to solving the standard Sturm–Liouville problem with third-type boundary conditions.

2. Nonlocal modal analysis

2.1 Basic equations

We consider a differentially rotating ideal fluid in a homogeneous vertical magnetic field. Classical results were obtained in papers by E Velikhov and S Chandrasekhar, who studied the stability of sheared hydromagnetic flows [6, 7].

The equations of motion of an ideal MHD fluid read:

(1) mass conservation equation

$$\frac{\partial \rho}{\partial t} + \nabla(\rho\,\mathbf{u}) = 0\,; \tag{1}$$

(2) Euler equation including gravity force and Lorentz force

$$\frac{\partial \mathbf{u}}{\partial t} + (\mathbf{u}\nabla)\,\mathbf{u} = -\frac{1}{\rho}\,\nabla p - \nabla\phi_{\mathrm{g}} + \frac{1}{4\pi\rho}\,(\nabla\times\mathbf{B})\times\mathbf{B} \tag{2}$$

(here, ϕ_{g} is the Newtonian gravitational potential [2]);

(3) induction equation

$$\frac{\partial \mathbf{B}}{\partial t} = \nabla\times(\mathbf{u}\times\mathbf{B})\,. \tag{3}$$

We will consider adiabatic perturbations with constant entropy

$$\frac{\partial s}{\partial t} + (\mathbf{u}\nabla)\,s = 0\,. \tag{4}$$

For such adiabatic perturbations, perturbed density variations are zero, $\rho_1 = 0$, and pressure variations in the energy equation vanish, $p_1 = 0$ (see, e.g., Appendix A in [26]).

We analyze the case of a purely Keplerian rotation where the unperturbed velocity is $v_\phi \equiv u_{\phi,0} = \sqrt{GM/r}$, $u_{r,0} = u_{z,0} = 0$. We assume that the forces caused by the pressure gradient are small and only appear in the perturbed equations.

2.2 Case of incompressible fluid

Let us consider small Eulerian perturbations in an ideal incompressible fluid. The velocity components in the back-

[2] In principle, one can solve the problem in the Schwarzschield metric using the potential $\phi = (c^2/2)\ln(1 - (r_{\mathrm{g}}/r))$, $r_{\mathrm{g}} = 2GM/c^2$ (see [25]).

ground undisturbed flow with velocity $u_{\phi,0}$ will be u_r, u_ϕ, u_z. The magnetic field can be expressed as $\mathbf{B} = \mathbf{B}_0 + \mathbf{b}$, and the pressure, as $p_0 + p_1$. We will consider the poloidal background field $\mathbf{B}_0$. We will seek perturbations in the form of $f(r)\exp[\mathrm{i}(\omega t - k_z z)]$, noting that time t and the coordinate z only appear in the system of equations through the derivative sign.

The choice of perturbations with harmonic functions in the vertical coordinate is dictated by the nature of the problem for disk flows that are confined by the z-coordinate. In such flows (accretion and protoplanetary disks, gas disks in galaxies), the vertical pressure gradient is balanced by the gradient of gravitational force along the z-coordinate, distinguishing them from laboratory flows.

The integration of the unperturbed Euler equation over the z-coordinate leads to a polytropic density distribution $\rho(r, z) = \rho_c(1 - (z/z_0)^2)^n$, with a semi-thickness of $z_0 = 2(n+1)P_c/(\Omega^2(r)\rho_c)$, where ρ_c and P_c are the central density and pressure, and n is the polytropic index ($n = 3/2$ for a convectively stable disk). For the polytropic equation of state, $n = 1/(\gamma - 1)$, where γ is the adiabatic index, and in the case of an incompressible fluid, $\gamma \to \infty$ and $n = 0$. In this limiting case, the vertical density gradient vanishes, and the model flow represents a Keplerian disk with a constant vertical density limited by the disk's semi-thickness h (Π-shaped density distribution). The density can vary radially (see Section 3).

For infinitesimal perturbations, the approximation of perturbations with harmonic functions in the z-coordinate is suitable for both thin disks ($h/r \ll 1$) and thick disks ($h/r \lesssim 1$), provided that the wavelength of the perturbations is smaller than the disk's half-thickness: $\lambda = 2\pi/k_z < h$. Therefore, the final equations for linear perturbations in the case of an incompressible fluid, which will be derived below, are no different from the equations for laboratory plasmas with a constant density along the z-coordinate.

For the chosen perturbations, the continuity equation (1) for an incompressible fluid, $\nabla\mathbf{u} = 0$, can be expressed in cylindrical coordinates as follows:

$$\frac{1}{r}\frac{\partial}{\partial r}(ru_r) - \mathrm{i}k_z u_z = \frac{\partial u_r}{\partial r} + \frac{u_r}{r} - \mathrm{i}k_z u_z = 0\,. \tag{5}$$

It should be noted that, in the local approximation, the small term u_r/r in the continuity equation is typically ignored. In this case, the perturbations can be sought in the form $\propto \exp[\mathrm{i}(\omega t - k_r r - k_z z)]$. The equation of magnetic field solenoidality, $\nabla\mathbf{B} = 0$, can be written in a similar manner:

$$\frac{1}{r}\frac{\partial}{\partial r}(rb_r) - \mathrm{i}k_z b_z = 0\,. \tag{6}$$

The radial, azimuthal, and vertical components of the Euler equation are, respectively,

$$\mathrm{i}\omega u_r - 2\Omega\, u_\phi = -\frac{1}{\rho_0}\frac{\partial p_1}{\partial r} - \frac{c_A^2}{B_0}\left[\frac{\partial b_z}{\partial r} + \mathrm{i}k_z b_r\right], \tag{7}$$

$$\mathrm{i}\omega u_\phi + \frac{\varkappa^2}{2\Omega}\,u_r = -\mathrm{i}\,\frac{c_A^2}{B_0}\,k_z b_\phi \tag{8}$$

(here, we introduced the epicyclic frequency $\varkappa^2 = 4\Omega^2 + r\,(\mathrm{d}\Omega^2/\mathrm{d}r) \equiv (1/r^3)\,\mathrm{d}(\Omega^2 r^4)/\mathrm{d}r$ and unperturbed Alfvén velocity $c_A^2 = B_0^2/(4\pi\rho_0)$),

$$\mathrm{i}\omega u_z = \mathrm{i}k_z\,\frac{p_1}{\rho_0}\,. \tag{9}$$

The three components of the induction equation, taking into account the solenoidality of the magnetic field $\nabla\mathbf{B} = 0$, read

$$\mathrm{i}\omega b_r = -\mathrm{i}B_0 k_z u_r\,, \tag{10}$$

$$\mathrm{i}\omega b_\phi = -\mathrm{i}B_0 k_z u_\phi + r\,\frac{\mathrm{d}\Omega}{\mathrm{d}r}\,b_r\,, \tag{11}$$

$$\mathrm{i}\omega b_z = -B_0\,\frac{1}{r}\,\frac{\partial r u_r}{\partial r}\,. \tag{12}$$

Let us express all perturbations in terms of the radial perturbations of the magnetic field b_r. Using Eqn (5), (9), and (10), we find

$$\frac{p_1}{\rho_0} = \frac{\omega u_z}{k_z} = \mathrm{i}\,\frac{\omega^2}{B_0 k_z^3}\,\frac{1}{r}\,\frac{\partial r b_r}{\partial r}\,. \tag{13}$$

From Eqn (10), we find

$$u_r = -\frac{\omega}{B_0 k_z}\,b_r\,. \tag{14}$$

Substituting (14), (11), and (6) into Eqn (8) yields

$$(c_A^2 k_z^2 - \omega^2)u_\phi = \mathrm{i}\left[\frac{\omega^2\varkappa^2}{2\Omega B_0 k_z} - \frac{c_A^2 k_z}{B_0}\,r\,\frac{\mathrm{d}\Omega}{\mathrm{d}r}\right]b_r\,. \tag{15}$$

Finally, using (13)–(15), from Eqn (7) we obtain a second-order differential equation for b_r:

$$\left(c_A^2 - \frac{\omega^2}{k_z^2}\right)^2\left[\frac{\partial^2 b_r}{\partial r^2} + \frac{\partial}{\partial r}\left(\frac{b_r}{r}\right) - b_r k_z^2\right] + 2\Omega\left(\frac{\omega^2}{k_z^2}\,\frac{\varkappa^2}{2\Omega} - c_A^2\,r\,\frac{\mathrm{d}\Omega}{\mathrm{d}r}\right)b_r = 0\,. \tag{16}$$

This equation should be complemented with boundary conditions, which are determined by the problem's formulation. For instance, E P Velikhov considered the flow between two rigid conducting cylinders, where the velocity and magnetic field perturbations were set to zero. In a more realistic scenario applicable to thin accretion disks, boundary conditions need to be chosen at the free boundary. For magnetized disks, various formulations of such boundary conditions are possible (see, for example, the discussion in [21]). We will demonstrate that the boundary conditions at the inner and outer edges of a Keplerian thin disk with a magnetic field correspond to the vanishing of Lagrangian variations of pressure. First, let us consider how a homogeneous magnetic field can be created in a thin conducting disk.

2.3 How to create a uniform magnetic field in a thin disk

Let us discuss how to create a uniform magnetic field in an accretion disk (Fig. 1). First, let us recall that this can be easily achieved in the case of two infinite well-conducting cylinders (Fig. 1a) with currents flowing in opposite directions. However, how can we organize currents in a flat conducting disk to obtain a uniform magnetic field inside it (Fig. 1b)? To answer this question, let us consider the following problem. Suppose we have a well-conducting sphere with surface currents $j_\phi \propto \sin\theta$ such that the field inside the sphere is uniform. We smoothly deform the sphere into a disk while preserving the magnetic flux $\mathrm{d}\Phi_s = B_0\cos\theta\,\mathrm{d}S$, where $\mathrm{d}S = 2\pi R_0^2\sin\theta\,\mathrm{d}\theta$ is an element of the surface area of the sphere, and θ is the angle between the surface normal and the

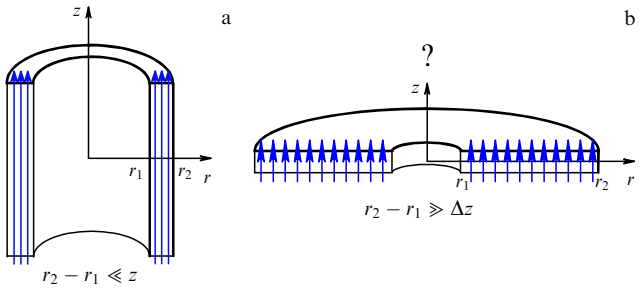

Figure 1. (a) Flow in a uniform magnetic field within a narrow gap between two cylinders. (b) Thin extended accretion disk in a uniform vertical magnetic field.

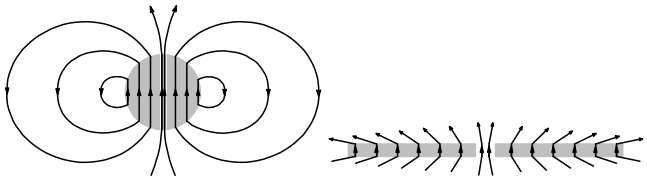

Figure 2. Deformation of a conducting sphere onto a disk. Surface Lorentz force $\mathbf{j}_s \times \mathbf{B}$ transforms the sphere into an elongated disk in the absence of other forces.

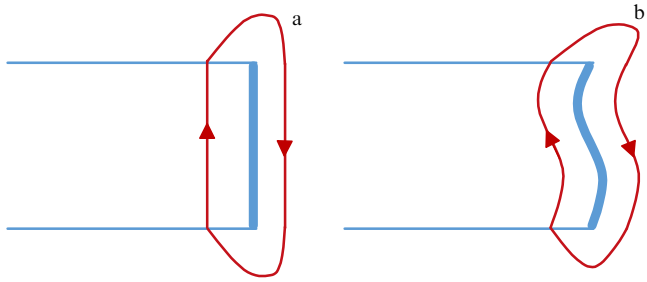

Figure 3. Schematic illustrating the cancellation of Lorentz force $\mathbf{j}_s \times \mathbf{B}$ at the outer boundary of the accretion disk. (a) Unperturbed configuration, with surface current $\mathbf{j}_s$ flowing perpendicular to the plane of the image. (b) Perturbed case, showing only the projection of the field onto the r, z plane. Perturbed component of the field b_ϕ is not shown.

magnetic field lines.In the disk, we have $\mathrm{d}\Phi_\mathrm{d} = B_\mathrm{d} 2\pi r\,\mathrm{d}r$ (B_d being the field in the disk). Preserving the flux $\Phi_s = \Phi_\mathrm{d}$ implies $2\pi R_0^2 \int B_0 \sin\theta\cos\theta\,\mathrm{d}\theta = 2\pi \int B_\mathrm{d} r\,\mathrm{d}r$. In the case of a uniform field, we have $R_0^2 B_0 \sin^2\theta + C = B_\mathrm{d} r^2$. The constant C must be zero to satisfy the condition $\theta \to 0$, $r \to 0$. For uniform fields and $\theta = \pi/2$, we find the radius of the outer disk: $r_\mathrm{d} = R_0\sqrt{B_0/B_\mathrm{d}}$. Thus, we have constructed a disk with surface currents that induce a bending of the magnetic field lines on the surface and a uniform magnetic field inside.

Now, let us remove a narrow region around the vertical axis from the considered sphere. Since the surface currents vanish near the vertical axis, removing a small region near the axis will not significantly alter the field inside the sphere. Of course, such an operation changes the topology: the sphere transforms into a torus.

Alternatively, the sphere can be deformed into a disk while preserving the magnetic flux, but with a radially variable magnetic field, $B_\mathrm{d}(r)$. During the deformation process, the changing magnetic field induces an electric field, which in turn strengthens or weakens the surface currents j_s (Fig. 2). It should be evident that, by deforming the sphere while conserving the magnetic flux, any desired dependence of the magnetic field on the radius can be obtained.

It is worth noting that, in the obtained configuration, the surface current on the inner boundary of the disk becomes zero, and, consequently, the Lorentz force acting on the surface element, $\mathbf{j}_s \times \mathbf{B}$, also vanishes. At the outer boundary, as the magnetic field changes sign when transitioning from the disk to the outside, there is a jump in the magnetic field, and a surface current must flow. The Lorentz force will be determined by the sum of two forces acting on the surface current from the inner and outer magnetic fields. Since, by construction, the outer and inner fields are equal but oppositely directed near the boundary, the total Lorentz force applied to the outer boundary of the disk will be zero (Fig. 3).

2.4 Differential equation for small perturbations

Following [6] and [7], it is straightforward to show that in Eqn (16) ω^2 must be a real number for a wide range of boundary conditions, i.e., only oscillations ($\omega^2 > 0$) or exponential growth or decay ($\omega^2 < 0$) of perturbations is allowed. It is convenient to eliminate the first derivative from (16) using the substitution $\Psi = b_r\sqrt{r}$ in order to obtain a second-order differential equation:

$$\frac{\mathrm{d}^2\Psi}{\mathrm{d}r^2} + \left\{-k_z^2 - \frac{3}{4}\frac{1}{r^2} + \frac{2\Omega\left[(\omega^2/k_z^2)\varkappa^2/(2\Omega) - c_\mathrm{A}^2 r\,(\mathrm{d}\Omega/\mathrm{d}r)\right]}{(c_\mathrm{A}^2 - \omega^2/k_z^2)^2}\right\} \times \Psi = 0\,. \tag{17}$$

The boundary conditions for this equation are selected based on physical considerations, ensuring that the Lagrangian pressure perturbations vanish on the free boundary (recall that, as shown earlier, the surface Lorentz force is zero on both boundaries):

$$\Delta p = \delta p + (\boldsymbol{\xi}\nabla)\,p = 0\,, \tag{18}$$

where $\boldsymbol{\xi}$ is the vector of infinitesimal displacement and $\delta p = p_1$ is the Eulerian pressure variation. Since, in our problem formulation, Keplerian unperturbed flow is assumed, in which the gravitational force is balanced by the centrifugal force, for small displacements $\boldsymbol{\xi}$, the second term in the expression for the Lagrangian variation can be disregarded (up to terms of order $(h/r)^2$ in a thin accretion disk with semi-thickness h), and $\Delta p = p_1$. After dividing by the differential of time $\mathrm{d}t$, equation (18) can be written as

$$\frac{\mathrm{D}p}{\mathrm{D}t} = \frac{\partial p}{\partial t} + (\mathbf{u}\nabla)\,p = 0\,,$$

where $\mathrm{D}/\mathrm{D}t$ represents the Lagrangian derivative, and $\partial/\partial t$ represents the Eulerian derivative.

At the outer and inner boundaries of the accretion disk with a magnetic field, the boundary conditions can be expressed as $p_1|_{r_\mathrm{in},\,r_\mathrm{out}} = 0$. As implied by Eqn (13), these boundary conditions lead to homogeneous third-type boundary conditions for the function Ψ at the flow boundaries r_in, r_out:

$$\left.\frac{\mathrm{d}\Psi}{\mathrm{d}r}\right|_{r_\mathrm{in}} + \frac{1}{2}\left.\frac{\Psi}{r}\right|_{r_\mathrm{in}} = 0, \quad \left.\frac{\mathrm{d}\Psi}{\mathrm{d}r}\right|_{r_\mathrm{out}} + \frac{1}{2}\left.\frac{\Psi}{r}\right|_{r_\mathrm{out}} = 0\,. \tag{19}$$

It is worth noting that, in E P Velikhov's work (see [6] and [22]), a boundary value problem with homogeneous first-type conditions at the boundaries ($\Psi|_{r_\mathrm{in}} = 0$, $\Psi|_{r_\mathrm{out}} = 0$) was considered.

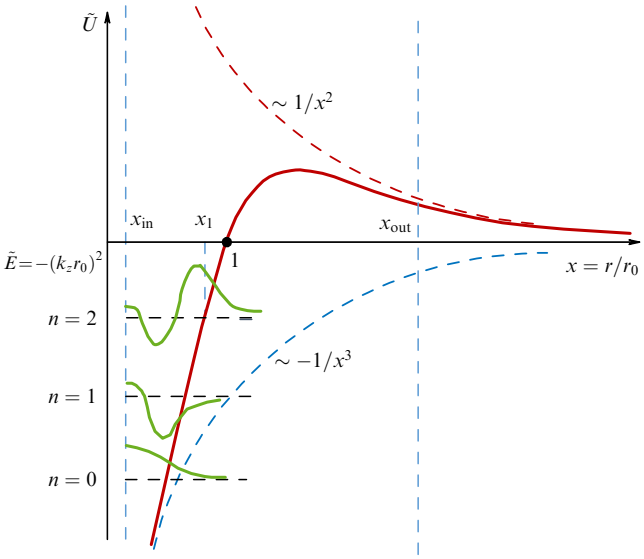

Figure 4. Schematic of effective potential $\tilde{U}$ with characteristic points $x_{\rm in}$ (inner boundary of the flow), x_1 (turning point in the potential for a given energy level), $x = 1$ (point where the potential becomes zero), and $x_{\rm out}$ (outer radius of the flow). First three energy levels ($n = 0, 1, 2$) and their corresponding eigenfunctions of the problem are shown in green color, where $x_{\rm out} > 1$.

Equation (17) can be interpreted as a Schrödinger-like equation with 'energy'

$$E = -k_z^2 \tag{20}$$

and 'potential'

$$U = \frac{3}{4}\frac{1}{r^2} - \frac{(\omega^2/k_z^2)\varkappa^2 - c_{\rm A}^2 r\,({\rm d}\Omega^2/{\rm d}r)}{(c_{\rm A}^2 - \omega^2/k_z^2)^2}\,. \tag{21}$$

As is well known (see, for example, [27, 28]), in the region of negative potential values U, there exist eigenvalues ('energy levels') with negative energy $E < 0$. The existence of levels with negative energy, i.e., solutions for **b**, for real k_z and $\omega^2 < 0$, indicates the instability of the flow. Thus, the form of the potential U determines the region in the flow and the range of values of **B** that allow the development of MRI.

Let us highlight the properties of potential U that are relevant to our problem. For the Keplerian law with $\Omega^2 = GM/r^3$ and $\varkappa^2 = \Omega^2$, the potential takes the form

$$U = \frac{3}{4}\frac{1}{r^2} - \frac{GM}{r^3}\,\frac{\omega^2/k_z^2 + 3c_{\rm A}^2}{(c_{\rm A}^2 - \omega^2/k_z^2)^2}\,. \tag{22}$$

For unstable modes ($\omega^2 < 0$), the numerator in the second term of equation (22) is positive only for perturbations with $\omega^2 > -3c_{\rm A}^2 k_z^2$. Otherwise, potential U is strictly positive, and there are no stable states with negative energy. For $\omega^2 < 0$, the denominator in equation (22) does not vanish. In our problem (Fig. 4), there are several characteristic points: the inner radius of the disk $r_{\rm in}$, the turning point r_1 for a given negative energy $E = -k_z^2$, the zero point of the potential r_0, and $r_{\max} = (3/2)r_0$, where the potential is maximal. It is evident that $r_{\rm in} \leqslant r_1 \leqslant r_0$.

The potential turns to zero at the point

$$r_0 = \frac{4}{3}\,GM\,\frac{\omega^2/k_z^2 + 3c_{\rm A}^2}{(c_{\rm A}^2 - \omega^2/k_z^2)^2} = \frac{4}{3}\,\frac{GM}{c_{\rm A}^2}\,\frac{\omega^2/(k_z^2 c_{\rm A}^2) + 3}{\left[1 - \omega^2/(k_z^2 c_{\rm A}^2)\right]^2}\,. \tag{23}$$

It is convenient to introduce a dimensionless variable $x = r/r_0$. Then, the dimensionless potential can be written as

$$\tilde{U} = U r_0^2 = \frac{3}{4}\frac{1}{x^2} - \frac{3}{4}\frac{1}{x^3}\,. \tag{24}$$

The dimensionless energy in the Schrödinger equation (17) is equal to

$$\tilde{E} = -k_z^2 r_0^2\,. \tag{25}$$

The turning point of the potential U is determined by the equation

$$-k_z^2 - U(r_1) = 0 \tag{26}$$

(see Fig. 4). Beyond the radius r_1, the perturbations decay quasiexponentially. In dimensionless units, the turning point $x_1 = r_1/r_0$ of the potential $\tilde{U}$ is determined by the equation

$$4\tilde{E}x_1^3 - 3x_1 + 3 = 0\,, \quad x_1 \leqslant 1\,. \tag{27}$$

For negative energy $\tilde{E}$, this cubic equation has one real root $x_1 = r_1/r_0 < 1$:

$$x_1 = \left(\frac{3}{-8\tilde{E}}\right)^{1/3}\left[\left(1 - \sqrt{1 - \frac{1}{9\tilde{E}}}\right)^{1/3} + \left(1 + \sqrt{1 - \frac{1}{9\tilde{E}}}\right)^{1/3}\right]. \tag{28}$$

Numerical solutions of Eqn (17) can be found in Appendix A. It should be noted that the global nonlocal analysis of MRI, leading to an equation of the form of one-dimensional Schrödinger Eqn (17), has been investigated by [21, 24] with different boundary conditions.

2.5 Derivation of the dispersion equation and critical Alfvén velocity

Thus, in dimensionless variables, the problem reduces to a Sturm–Liouville problem for the equation

$$\Psi'' - \tilde{U}\,\Psi + \tilde{E}\,\Psi = 0 \tag{29}$$

with the potential (24) and boundary conditions

$$\left.\frac{{\rm d}\Psi}{{\rm d}x}\right|_{x_{\rm in}} + \frac{1}{2}\left.\frac{\Psi}{x}\right|_{x_{\rm in}} = 0\,, \quad \left.\frac{{\rm d}\Psi}{{\rm d}x}\right|_{x_{\rm out}} + \frac{1}{2}\left.\frac{\Psi}{x}\right|_{x_{\rm out}} = 0\,. \tag{30}$$

Since potential $\tilde{U}$ changes sign at $x = 1$ ($r = r_0$), when solving this problem, it is necessary to distinguish between two cases: (1) the outer radius of the flow is located beyond the zero point of the potential $x_{\rm out} > 1$ ($r_{\rm out} > r_0$), and (2) the flow terminates before reaching the zero point of the potential $x_{\rm out} < 1$ ($r_{\rm out} < r_0$) (see details in Appendices A and B, respectively). From the solution of the boundary value problem, a discrete set of eigenvalues $\tilde{E}_n$, $n = 0, 1, 2, \ldots$, is obtained:

$$\tilde{E}_n = -k_z^2 r_0^2\,. \tag{31}$$

In the case of $x_{\rm out} > 1$, the number n corresponds to the number of zeros of the eigenfunctions in the interval between the inner boundary and the turning point of the potential for a given level $[x_{\rm in}, x_1(\tilde{E}_n)]$.

From Eqn (31), for each level with negative energy $\tilde{E}_n$, we obtain a dispersion equation

$$r_0 = \frac{\sqrt{-\tilde{E}_n}}{k_z} = \frac{4}{3}\,\frac{GM}{c_A^2}\,\frac{\omega^2/(k_z^2 c_A^2) + 3}{\left[1 - \omega^2/(k_z^2 c_A^2)\right]^2}\,. \tag{32}$$

In dimensionless units normalized by r_0, Eqn (32) becomes a quadratic equation for the dimensionless quantity $\omega^2/(k_z^2 c_A^2)$:

$$\frac{3}{4}\left(\frac{c_A}{v_\phi(r_0)}\right)^2\left(1 - \frac{\omega^2}{k_z^2 c_A^2}\right)^2 - \frac{\omega^2}{k_z^2 c_A^2} - 3 = 0\,,$$

$$v_\phi^2(r_0) \equiv \frac{GM}{r_0} = \frac{GMk_z}{\sqrt{-\tilde{E}_n}}\,. \tag{33}$$

Its solution is as follows:

$$\omega^2 = c_A^2 k_z^2\left(1 + \frac{1 \pm \sqrt{1 + 12\left[c_A/v_\phi(r_0)\right]^2}}{(3/2)\left[c_A/v_\phi(r_0)\right]^2}\right). \tag{34}$$

Note that this dispersion equation involves the flow velocity at radius r_0 and does not explicitly depend on the boundaries of the flow where the boundary conditions are satisfied; the boundary conditions determine the set of eigenvalues $\tilde{E}_n$.

The critical magnetic field corresponding to the neutral mode $\omega^2 = 0$ is given by

$$\left(\frac{c_A}{v_\phi(r_0)}\right)_{cr}^2 = 4\,, \tag{35}$$

which can be rewritten as

$$(c_A)_{cr}^2 = \frac{4GM}{r_0} = \frac{4GMk_z}{\sqrt{-\tilde{E}_n}}\,. \tag{36}$$

Thus, in a sufficiently strong magnetic field, the shear flow is stabilized by the Lorentz force ($\omega^2 = 0$), as first noted in [6] for flow in a narrow gap between two conducting cylinders.

Using Eqn (35), we rewrite Eqn (34) in the form

$$\frac{\omega^2}{(c_A)_{cr}^2 k_z^2} = \left(\frac{c_A}{(c_A)_{cr}}\right)^2\left(1 + \frac{1 \pm \sqrt{1 + 48\left(c_A/(c_A)_{cr}\right)^2}}{6\left(c_A/(c_A)_{cr}\right)^2}\right). \tag{37}$$

Below, only the unstable modes with $\omega^2 < 0$ are considered, corresponding to the minus sign in Eqn (37). For small $\left(c_A/(c_A)_{cr}\right)^2 \ll 1$, Eqn (37) can be approximated as

$$\frac{\omega^2}{(c_A)_{cr}^2 k_z^2} \approx \left(\frac{c_A}{(c_A)_{cr}}\right)^2\left[-3 + 48\left(\frac{c_A}{(c_A)_{cr}}\right)^2\right]. \tag{38}$$

In other words, $\omega^2 \to 0$ as $c_A^2 \to 0$. This behavior of ω^2 differs from the result of local analysis, where the MRI occurs even for an arbitrarily small (but nonzero!) background magnetic field (see, for example, [26]).

It is evident that there is a maximum growth rate of the MRI and its corresponding Alfvén speed (Fig. 5):

$$\left(\frac{c_A}{(c_A)_{cr}}\right)_{max}^2 = \frac{5}{16}\,, \qquad \frac{\omega_{max}^2}{(c_A)_{cr}^2 k_z^2} = -\frac{3}{16}\,. \tag{39}$$

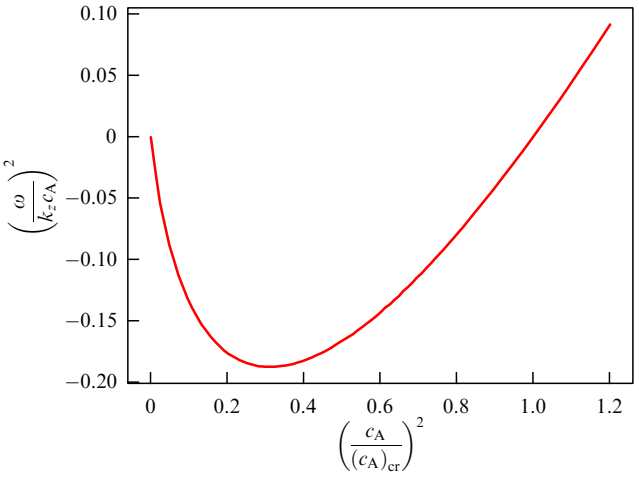

Figure 5. Solution of dispersion equation (37) with a minus sign in front of the square root for unstable modes $\omega^2 < 0$.

In real flows, there is always an inner radius r_{in}. For sufficiently large outer radius $r_{out} \gg r_{in}$, it is possible to solve the problem exactly and find the eigenvalues $\tilde{E}_n = -k_z^2 r_0^2$ (see Appendix A), from which the location of the zero point r_0 of the effective potential $U(r)$ can be calculated. In the quasiclassical approximation, the solution $\tilde{E}_n(x_{in})$, where $x_{in} = r_{in}/r_0$, is expressed through integral (85) (see Appendix A). Then, the position of r_0 in the flow can be calculated from the solution to the problem with a given r_{in} using the formula $r_0 = r_{in}/x_{in}$. In the special case of small $k_z \approx 0$ (i.e., $\tilde{E}_n \approx 0$), there is an analytical solution (see (87), (88)):

$$r_0 = r_{in}\left\{\left[\frac{\pi}{\sqrt{3}}\left(n + \frac{3}{4}\right) + \frac{\pi}{2}\right]^2 + 1\right\}. \tag{40}$$

In the case of $r_{out} < r_0$, the potential between the boundaries does not change sign, and the problem of finding the eigenvalues of Eqn (29) is simplified (see Appendix B).

2.6 Application to thin accretion disks

In accretion disks, the wavelength of perturbations $\lambda = 2\pi/k_z$ in the vertical coordinate must be smaller than the disk semi-thickness h. This condition limits the allowed 'energy levels.' Indeed, at the turning point x_1, we have

$$\tilde{E} = -k_z^2 r_0^2 = -4\pi^2\left(\frac{h}{\lambda}\right)^2\left(\frac{r_1}{h}\right)^2\frac{1}{x_1^2}\,. \tag{41}$$

Therefore, the requirement

$$\left(\frac{\lambda}{h}\right)^2 = -\frac{4\pi^2}{x_1^2\tilde{E}}\left(\frac{r_1}{h}\right)^2 < 1 \tag{42}$$

gives the permissible energy levels that satisfy the following condition:

$$x_1^2|\tilde{E}| > \frac{4\pi^2}{(h/r_1)^2}\,. \tag{43}$$

For a typical value of the relative thickness of a geometrically thin disk, $h/r \lesssim 0.1$, in thin accretion disks, this yields $x_1^2|\tilde{E}| > 4 \times 10^3$. Considering that, for large $|\tilde{E}| \gg 1$, $x_1 \approx (3/(4|\tilde{E}|))^{1/3}$ (see Eqn (28)), the corresponding energy

levels must have $|\tilde{E}| > 7 \times 10^{10}$. Such levels are only possible for very small $x_{\rm in} \ll 1$ (see Appendix A, Fig. 13).

The critical magnetic field, above which the MRI is suppressed, can be expressed in terms of the Keplerian velocity at the inner boundary of the flow, $v_\phi(r_{\rm in})$:

$$(c_{\rm A})^2_{\rm cr} = \frac{4GM}{r_0} = x_{\rm in}\,\frac{4GM}{r_{\rm in}} = 4x_{\rm in} v_\phi^2\,(r_{\rm in})\,. \tag{44}$$

It is easy to obtain an upper limit on the possible value of the dimensionless parameter $x_{\rm in} = r_{\rm in}/r_0$. Indeed, all possible energy levels can take values

$$-\tilde{E}_n = \frac{r_{\rm in}^2\,k_z^2}{x_{\rm in}^2} < -\tilde{U}(x_{\rm in}) = \frac{3}{4}\,\frac{1}{x_{\rm in}^3} - \frac{3}{4}\,\frac{1}{x_{\rm in}^2}\,, \tag{45}$$

from which

$$x_{\rm in} < \frac{1}{1 + (4/3)\,r_{\rm in}^2\,k_z^2}\,. \tag{46}$$

Note that this inequality (46) gives an obvious upper limit $x_{\rm in} < 1$ for $k_z \to 0$, while, as shown in Appendix A, energy levels with $n = 0$ exist only when $x_{\rm in} < 0.8116$. Substituting inequality (46) into (44), we obtain an upper limit for the critical magnetic field:

$$(c_{\rm A})^2_{\rm cr} < \frac{4v_\phi^2\,(r_{\rm in})}{1 + (4/3)\,r_{\rm in}^2\,k_z^2}\,. \tag{47}$$

Using the condition for thin disks with the wavelength of perturbations in the z-coordinate $\lambda/h = 2\pi/(k_z h) < 1$ and considering $h/r_{\rm in} < 1$, we transform (47) into the form

$$\frac{(c_{\rm A})_{\rm cr}}{v_\phi(r_{\rm in})} < \frac{\sqrt{3}}{2\pi}\left(\frac{h}{r_{\rm in}}\right)\sqrt{\frac{\lambda}{h}}, \quad \frac{(c_{\rm A})_{\rm cr}}{c_{\rm s}(r_{\rm in})} < \frac{\sqrt{3}}{2\pi}\,\sqrt{\frac{\lambda}{h}}. \tag{48}$$

(In the last inequality, we used the relation between the Keplerian velocity and the sound speed at the inner boundary of the thin accretion disk $c_{\rm s}(r_{\rm in}) = v_\phi(r_{\rm in})(h/r_{\rm in})$.)

Thus, in thin accretion disks, MRI perturbations with a wavelength $\lambda < h$ in the z-coordinate can be significantly suppressed.

Depending on the type of accretor (regular stars or relativistic compact objects), the inner radius of the flow can vary greatly from a few ten to millions of kilometers, while the outer radius is determined by the physical situation, such as being limited by the size of the Roche lobe in the case of binary systems. Since in thin disks $h/r \sim 0.05$, the upper limit of the critical magnetic field that suppresses MRI in thin disks (48) is $\sim 1/\sqrt{r_{\rm in}}$ and significantly differs for different types of accretors.

Previous studies on the critical magnetic field for suppressing MRI in the context of global analysis with different boundary conditions can be found, for example, in [18, 22]. In [18], the critical magnetic field was derived using the energy method. Only an upper estimate was obtained, according to which (equation (41) in the cited work) the critical magnetic field in thin disks is determined by the Alfvén velocity, which is equal to the Keplerian velocity of the flow multiplied by the square root of the ratio of the disk's semi-thickness to its radius. It should also be noted that the critical Alfvén velocity in the local analysis by [10] is, to within a multiplicative factor, equal to the Keplerian velocity multiplied by the ratio of the wavelength of a perturbation in the z-coordinate to the radius. As can be seen from a comparison of these statements with (48), our result provides a much more definite value for the critical field.

3. Magnetorotational instability with radially dependent Alfvén velocity

Until now, our consideration of MRI has been limited to the case of a constant background Alfvén velocity. However, in real astrophysical situations, the Alfvén velocity should decrease with radius as fast as the angular velocity of the flow or even faster. Below, we will consider two cases: (1) $c_{\rm A}^2$ depends on radius as $v_\phi^2 \propto 1/r$ due to the variable density with a constant background magnetic field, and (2) $c_{\rm A}^2 \propto 1/r^q$ for a variable background magnetic field with the density constant over radius.

3.1 Case of constant background magnetic field

The square of the Alfvén velocity can decrease linearly with radius when the background magnetic field is constant, but the density of the flow increases *linearly with radius*. It should be noted that the density varying with radius still implies the use of the continuity equation in the form of Eqn (5). Let us rewrite Eqn (1) as follows:

$$\frac{1}{\rho}\left(\frac{\partial\rho}{\partial t} + \mathbf{u}\nabla\rho\right) + \nabla\mathbf{u} = \frac{\mathrm{D}}{\mathrm{D}t}\ln\rho + \nabla\mathbf{u} = 0\,.$$

Now, locally, density ρ varies (Eulerian derivative $\partial\rho/\partial t \neq 0$), but the substantial (Lagrangian) derivative of density with time $\mathrm{D}\rho/\mathrm{D}t = \partial\rho/\partial t + \mathbf{u}\nabla\rho = 0$, $\mathrm{D}\ln\rho/\mathrm{D}t = 0$. Thus, for an incompressible fluid in the case of density varying with coordinates, the continuity equation becomes $\nabla\mathbf{u} = 0$ [29, 30]. Therefore, for a variable background density ρ_0, equations (5)–(12) for linear perturbations remain unchanged. However, instead of the potential Eqn (22) with $c_{\rm A}^2 = \text{const}$, the effective potential takes the form

$$\begin{aligned} U_e &= \frac{3}{4}\,\frac{1}{r^2} - \frac{GM}{r^3 c_{\rm A}^2}\,\frac{\omega^2/(k_z^2 c_{\rm A}^2) + 3}{\left[1 - \omega^2/(k_z^2 c_{\rm A}^2)\right]^2} \\ &= \frac{3}{4}\,\frac{1}{r^2} - \frac{GM}{r^3}\,\frac{\omega^2/k_z^2 + 3\epsilon v_\phi^2(r)}{\left[\epsilon v_\phi^2(r) - \omega^2/k_z^2\right]^2}\,. \end{aligned} \tag{49}$$

Here, $\epsilon \equiv c_{\rm A}^2/v_\phi^2 = \text{const}$ is a parameter. The potential (49) has the same characteristic points as in the previous case (see Section 2.4): r_0, where $U_e(r_0) = 0$, the turning point r_1, where $E - U_e(r_1) = 0$, and the inner radius of the flow $r_{\rm in}$.

The potential U_e becomes zero at the point

$$r_0 = \frac{4}{3}\,GM\,\frac{\omega^2/k_z^2 + 3\epsilon v_\phi^2\,(r_0)}{\left[\epsilon v_\phi^2\,(r_0) - \omega^2/k_z^2\right]^2}\,. \tag{50}$$

From the last equation, we obtain the dispersion equation $\omega(k_z)$:

$$\frac{3}{4}\,\epsilon\left(1 - \frac{\omega^2}{k_z^2\,\epsilon v_\phi^2\,(r_0)}\right)^2 - \frac{\omega^2}{k_z^2\,\epsilon v_\phi^2\,(r_0)} - 3 = 0 \tag{51}$$

with the solution

$$\omega^2 = \epsilon v_\phi^2\,(r_0)\,k_z^2\left(1 + \frac{1 \pm \sqrt{1 + 12\epsilon}}{3\epsilon/2}\right). \tag{52}$$

The unstable MRI mode corresponds to the minus sign before the square root. As in Section 2.5, the critical magnetic field corresponds to the neutral mode $\omega^2 = 0$:

$$\epsilon_{\rm cr} = \left(\frac{c_{\rm A}(r_0)}{v_\phi(r_0)}\right)^2 = 4\,. \tag{53}$$

For small $\epsilon \ll 1$,

$$\omega^2 \approx \epsilon v_\phi^2(r_0)\, k_z^2(-3+12\epsilon)\,. \tag{54}$$

It can be seen that Eqn (52) yields the same maximum growth rate of MRI and the corresponding value of the Alfvén velocity as before (cf. Eqn (39)):

$$\epsilon = \left(\frac{c_{\rm A}(r_0)}{v_\phi(r_0)}\right)^2_{\rm max} = \frac{5}{4}\,, \qquad \omega^2_{\rm max} = -\frac{3}{4}\,k_z^2\, v_\phi^2\,(r_0)\,. \tag{55}$$

Clearly, the critical Alfvén velocity is the same as derived earlier (see Eqn (35)).

Let us now consider the turning point r_1 in the potential U_e, determined by the equation $-k_z^2 - U_e(r_1) = 0$. In dimensionless variables $\tilde{E} = -k_z^2 r_0^2$ and $x = r/r_0$, the equation for x_1 reads

$$\tilde{E} - \tilde{U}_e = \tilde{E} - \frac{3}{4}\,\frac{1}{x_1^2} + \frac{1}{\epsilon x_1^2}\,\frac{3 + x_1\,K(\epsilon)}{\left[1 - x_1\,K(\epsilon)\right]^2} = 0\,, \tag{56}$$

where

$$K(\epsilon) = \frac{\omega^2}{k_z^2 c_{\rm A}^2(r_0)} = 1 + \frac{1-\sqrt{1+12\epsilon}}{3\epsilon/2}\,. \tag{57}$$

It should be noted that the 'attractive' part of the potential in Eqn (56) depends on the parameter ϵ. Also, in this case, for small $x \ll 1$, the 'repulsive' potential behaves as $1/x^2$ compared to $1/x^3$ in the case of Eqn (24). Equation (56) is a fourth-degree equation for x_1 (in contrast to the cubic equation, Eqn (27), for x_1 in the case of constant $c_{\rm A}^2$). For small $x_1 \ll 1$, the solution takes the form

$$x_1^2 \approx -\frac{3}{\tilde{E}}\left(\frac{1}{4} + \frac{1}{\epsilon}\right) \tag{58}$$

(cf. Eqn (28) for constant Alfvén velocity).

3.2 Case of radially dependent background magnetic field

If the background magnetic field depends on the radius, $\mathbf{B} = (0, 0, B_z(r))$, the linearized MHD equations become more complex. The radial and vertical components of Euler equations (7) and (9) are now expressed as follows, respectively:

$$\mathrm{i}\omega u_r - 2\Omega u_\phi = -\frac{1}{\rho_0}\,\frac{\partial p_1}{\partial r} - \frac{1}{4\pi\rho_0}\left[\frac{\partial(b_z B_z)}{\partial r} + \mathrm{i}k_z b_r B_z\right], \tag{59}$$

$$\mathrm{i}\omega u_z = \mathrm{i}k_z\frac{p_1}{\rho_0} + \frac{1}{4\pi\rho_0}\,b_r\,\frac{\partial B_z}{\partial r}\,. \tag{60}$$

The vertical component of the induction equation (12) turns into

$$\mathrm{i}\omega b_z = -\frac{1}{r}\,\frac{\partial(r u_r B_z)}{\partial r}\,. \tag{61}$$

Following a similar procedure as in Section 2.4, after some algebraic manipulations, we obtain the equation for b_r in the form

$$\begin{aligned}
&\left(c_{\rm A}^2 - \frac{\omega^2}{k_z^2}\right)\left[\frac{\partial^2 b_r}{\partial r^2} + \frac{\partial}{\partial r}\left(\frac{b_r}{r}\right) - b_r k_z^2\right] \\
&+ \frac{2\Omega\left[\omega^2\varkappa^2/(2\Omega k_z^2) - c_{\rm A}^2 r\left(\mathrm{d}\Omega/\mathrm{d}r\right)\right]}{c_{\rm A}^2 - \omega^2/k_z^2}\,b_r \\
&= \frac{\partial c_{\rm A}^2}{\partial r}\left\{-\frac{b_r}{2r} - \frac{1}{2}\,\frac{\partial b_r}{\partial r} + \frac{\omega^2}{k_z^2 c_{\rm A}^2}\right. \\
&\left.\times\left[-\frac{b_r}{2r} - \frac{\partial b_r}{\partial r} - \frac{1}{2}\,\frac{\partial^2 c_{\rm A}^2/\partial r^2}{\partial c_{\rm A}^2/\partial r}\,b_r + \frac{3}{4c_{\rm A}^2}\,\frac{\partial c_{\rm A}^2}{\partial r}\,b_r\right]\right\}.
\end{aligned} \tag{62}$$

The r.h.s. of the above equation vanishes for $c_{\rm A}^2 = \text{const}$. Here, we will consider the case of a power-law dependence of the Alfvén velocity on radius. Substituting $c_{\rm A}^2 \propto r^{-q}$ into Eqn (62), we obtain, for Keplerian flow ($\varkappa^2 = \Omega^2 = GM/r^3$), the following expression:

$$\begin{aligned}
&\frac{\partial^2 b_r}{\partial r^2} + \left[1 - q\,\frac{c_{\rm A}^2/2 + \omega^2/k_z^2}{c_{\rm A}^2 - \omega^2/k_z^2}\right]\frac{\partial}{\partial r}\left(\frac{b_r}{r}\right) \\
&\quad + b_r\left\{-k_z^2 + \frac{GM}{r^3}\,\frac{\omega^2/k_z^2 + 3c_{\rm A}^2}{\left(c_{\rm A}^2 - \omega^2/k_z^2\right)^2}\right. \\
&\quad \left. + \frac{q}{r^2}\,\frac{(-q/4-1)\,\omega^2/k_z^2 - c_{\rm A}^2}{c_{\rm A}^2 - \omega^2/k_z^2}\right\} = 0\,.
\end{aligned} \tag{63}$$

Equation (63) can be rewritten as

$$b_r'' + g(r)\,b_r' + f(r) = 0\,, \tag{64}$$

$$g(r) = \frac{1}{r}\,\frac{1 - q/2 - (q+1)\left(\omega^2/(k_z^2 c_{\rm A}^2)\right)}{1 - \omega^2/(k_z^2 c_{\rm A}^2)}\,, \tag{65}$$

$$\begin{aligned}
f(r) &= -k_z^2 + \frac{GM}{c_{\rm A}^2 r^3}\,\frac{\omega^2/(k_z^2 c_{\rm A}^2) + 3}{\left[1 - \omega^2/(k_z^2 c_{\rm A}^2)\right]^2} \\
&\quad - \frac{g(r)}{r} + \frac{q}{r^2}\,\frac{(-q/4-1)\,\omega^2/(k_z^2 c_{\rm A}^2) - 1}{1 - \omega^2/(k_z^2 c_{\rm A}^2)}\,.
\end{aligned} \tag{66}$$

The first derivative can be excluded in a standard way by the substitution $z = b_r \exp\left[-1/2\int^r g(s)\,\mathrm{d}s\right]$, yielding the equation

$$z'' + \left(f - \frac{g'}{2} - \frac{g^2}{4}\right)z = 0\,. \tag{67}$$

Substituting the functions f and g into Eqn (67), we obtain the equation

$$\begin{aligned}
z'' + \left\{-k_z^2 - \frac{3}{4}\,\frac{1}{r^2} - \frac{q}{r^2}\,\frac{q/16 + 1/2 - (q/4+1/2)\omega^2/(k_z^2 c_{\rm A}^2)}{\left[1 - \omega^2/(k_z^2 c_{\rm A}^2)\right]^2}\right. \\
\left. + \frac{GM}{c_{\rm A}^2 r^3}\,\frac{\omega^2/(k_z^2 c_{\rm A}^2) + 3}{\left[1 - \omega^2/(k_z^2 c_{\rm A}^2)\right]^2}\right\} z = 0\,.
\end{aligned} \tag{68}$$

Clearly, it reduces to Eqn (17) for $q = 0$ for the case of a constant magnetic field. When $q \neq 0$, the effective potential in the Schrödinger-like Eqn (68) reads

$$\begin{aligned}
U_q &= \frac{3}{4}\,\frac{1}{r^2} + \frac{q}{r^2}\,\frac{q/16 + 1/2 - \omega^2/(k_z^2 c_{\rm A}^2)(q/4+1/2)}{\left[1 - \omega^2/(k_z^2 c_{\rm A}^2)\right]^2} \\
&\quad - \frac{GM}{c_{\rm A}^2 r^3}\,\frac{\omega^2/(k_z^2 c_{\rm A}^2) + 3}{\left[1 - \omega^2/(k_z^2 c_{\rm A}^2)\right]^2}\,.
\end{aligned} \tag{69}$$

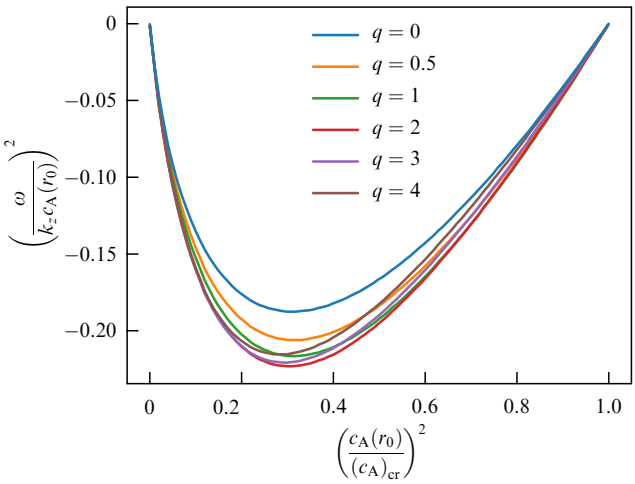

Figure 6. MRI dispersion curves described by Eqn (74) for various values of q. In the limit of $c_A/(c_A)_{cr} \ll 1$, the dispersion equation takes the form of Eqn (38) for all values of q.

For each value of q, the potential U_q becomes zero at

$$r_0 = \frac{GM}{c_A^2} \times \frac{\omega^2/(k_z^2 c_A^2) + 3}{(3/4)\left[1-\omega^2/(k_z^2 c_A^2)\right]^2 - (q^2/4+q/2)\omega^2/(k_z^2 c_A^2) + (q^2/16+q/2)}. \tag{70}$$

The dispersion equation at the point r_0 reads

$$\frac{\omega^2}{k_z^2 c_A^2(r_0)} = 1 + \frac{q}{3} + \frac{q^2}{6} + \frac{2}{3}\left(\frac{v_\phi(r_0)}{c_A(r_0)}\right)^2 \pm \sqrt{\left(\frac{q^2}{6} + \frac{q}{3} + \frac{2}{3}\left(\frac{v_\phi(r_0)}{c_A(r_0)}\right)^2\right)^2 + \frac{16}{3}\left(\frac{v_\phi(r_0)}{c_A(r_0)}\right)^2 + \frac{q^2}{4}}. \tag{71}$$

The unstable MRI mode corresponds to the minus sign before the square root. The zero mode $\omega^2 = 0$ occurs at the critical magnetic field

$$\epsilon_{cr} \equiv \left(\frac{c_A(r_0)}{v_\phi(r_0)}\right)^2_{cr} = \frac{48}{12 + 8q + q^2}. \tag{72}$$

Using the identity

$$\left(\frac{v_\phi}{c_A}\right)^2 = \left(\frac{v_\phi}{(c_A)_{cr}}\right)^2 \left(\frac{(c_A)_{cr}}{c_A}\right)^2, \tag{73}$$

we rewrite the dispersion equation (71) in a form similar to Eqn (37), as a function of a dimensionless value $((c_A)_{cr}/c_A)^2$:

$$\frac{\omega^2}{(c_A)_{cr}^2 k_z^2} = \left(\frac{c_A}{(c_A)_{cr}}\right)^2 \left[1 + \frac{q}{3} + \frac{q^2}{6} + \frac{2}{3}\left(\frac{v_\phi}{c_A}\right)^2 \pm \sqrt{\left(\frac{q^2}{6} + \frac{q}{3} + \frac{2}{3}\left(\frac{v_\phi}{c_A}\right)^2\right)^2 + \frac{16}{3}\left(\frac{v_\phi}{c_A}\right)^2 + \frac{q^2}{4}}\right] \tag{74}$$

(see Fig. 6). In Eqn (74), value $(v_\phi/c_A)^2$ can be expressed in terms of Eqns (72) and (73).

Let us use, as above, the dimensionless variables $x = r/r_0$, $c_A^2 = c_A^2(r_0) x^{-q}$, and the parameter $\epsilon = c_A^2(r_0)/v_\phi^2(r_0)$ and denote the r.h.s. of Eqn (71) as $\omega^2/(k_z^2 c_A^2(r_0)) = K(\epsilon)$. Then, the dimensionless potential $\tilde{U}_q = U_q r_0^2$ is as follows:

$$\tilde{U}_q(x,\epsilon,q) = \frac{1}{x^2}\left(\frac{3}{4} + \frac{q^2/16 + q/2 - K(\epsilon)x^q(q^2/4+q/2)}{\left(1-K(\epsilon)x^q\right)^2}\right) - \frac{1}{x^{3-q}}\frac{3+K(\epsilon)x^q}{\epsilon\left(1-K(\epsilon)x^q\right)^2}. \tag{75}$$

It should be noted that, in the case of $q \neq 0$, both the 'repulsive' and 'attractive' parts of the effective potential depend on ϵ.

Let us discuss some features of the potential $\tilde{U}_q$.

(1) By construction, $\tilde{U}_q(1,\epsilon,q) = 0$ for any ϵ, q.

(2) For $\epsilon \to \epsilon_{cr}$, see Eqn (72), $K(\epsilon) \to 0$:

$$\tilde{U}_q(x, \epsilon \to \epsilon_{cr}, q) = \left(\frac{3}{4} + \frac{q^2}{16} + \frac{q}{2}\right)\left(\frac{1}{x^2} - \frac{1}{x^{3-q}}\right). \tag{76}$$

The potential $\tilde{U}_q(x, \epsilon \to \epsilon_{cr}, q = 1) = 0$ for any x. For $q < 1$, $\tilde{U}_q$ changes sign from negative to positive at $x = 1$, and vice versa for $q > 1$.

(3) For $q < 1$, only one zero point of the potential exists: $\tilde{U}_q(x = 1, \epsilon, q < 1) = 0$.

(4) For $q > 1$, the second zero point x_2 appears at $x < 1$ with $\lim_{\epsilon\to 0} x_2 = 0$ and $\lim_{x\to 0} \tilde{U}_q(x,\epsilon,q) \to +\infty$. That is, the potential reaches a minimum at a certain point x_{min}: $x_2 < x_{min} < 1$.

These features of the effective potential $\tilde{U}_q$ for different values of q and ϵ are shown in Figs 7–11. It can be seen that, for $q \leqslant 1$, the effective potential $\tilde{U}_q$ has the same shape as for

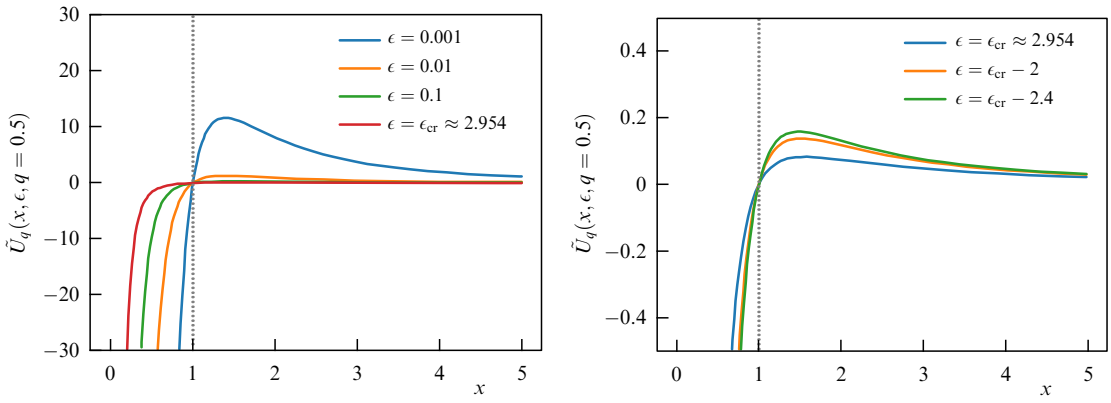

Figure 7. Effective potential $\tilde{U}_q(x,\epsilon,q)$ described by Eqn (75) for $q = 0.5$ and various values of parameter $\epsilon = c_A^2(r_0)/v_\phi^2(r_0)$. Critical value ϵ_{cr} is determined from Eqn (72).

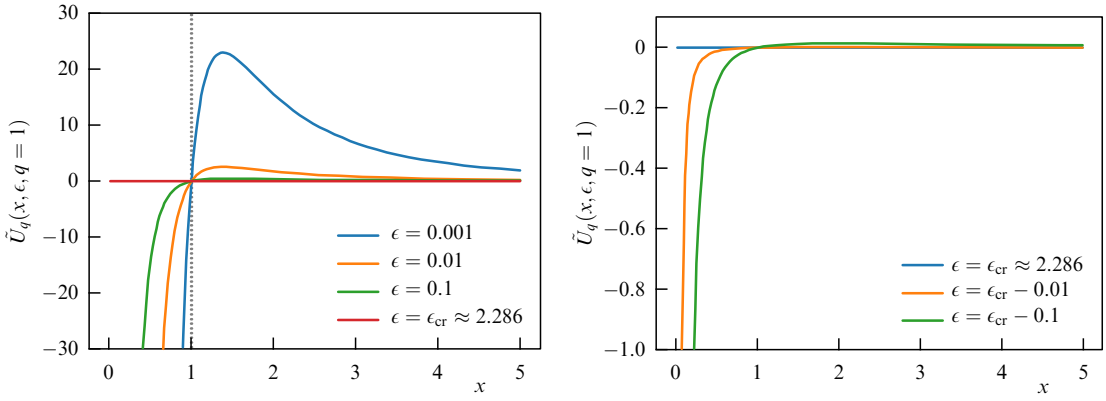

Figure 8. The same as in Fig. 7, for $q = 1$.

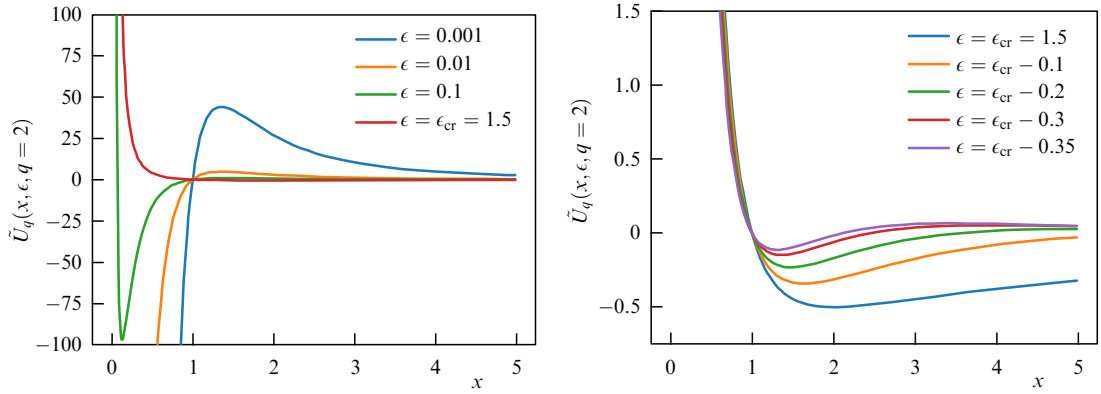

Figure 9. The same as in Fig. 7, for $q = 2$. Note the appearance of the second zero point of the potential as parameter ϵ decreases.

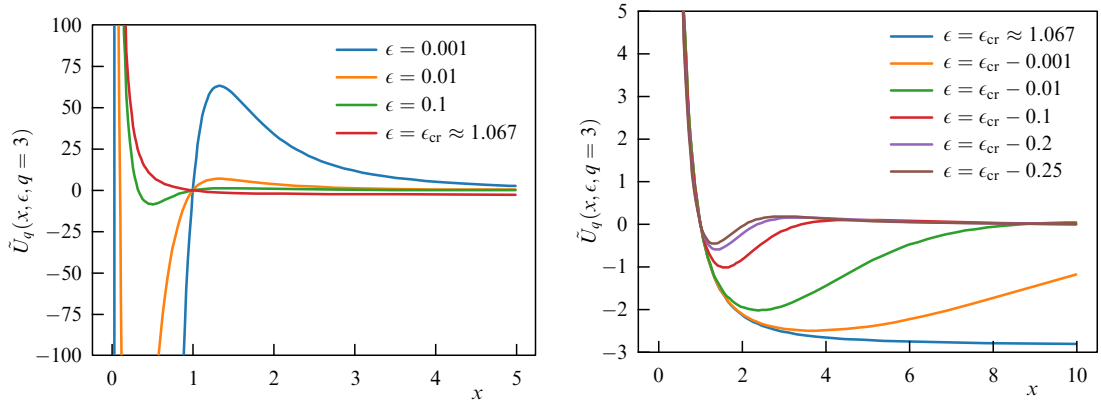

Figure 10. The same as in Fig. 7, for $q = 3$.

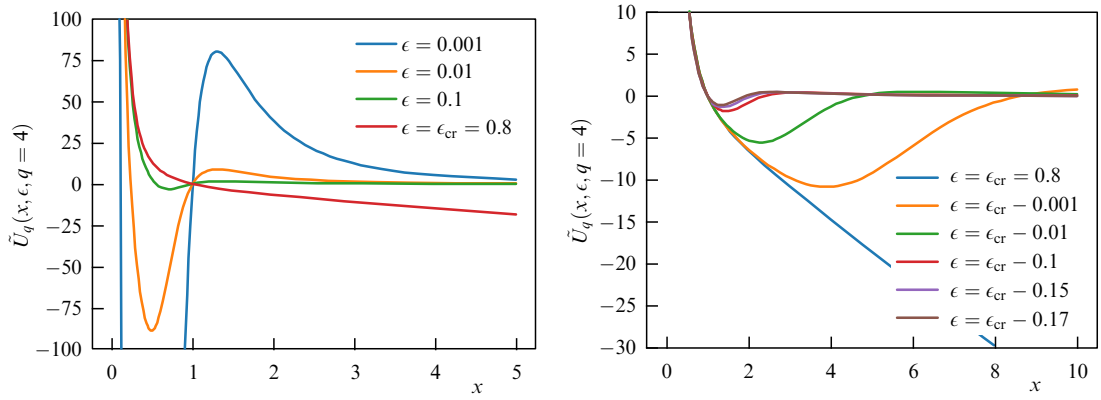

Figure 11. The same as in Fig. 7, for $q = 4$.

$q = 0$ (see Fig. 4), and the analysis of the MRI modes remains unchanged. For $q > 1$, a minimum of the effective potential appears with $x_2 < x_{\min} < 1$, and the unstable energy levels should be sought between the two turning points for the corresponding effective energies $\tilde{E} = -k_z r_0^2$. In contrast to the $q = 0$ case, a minimum energy $\tilde{E}_{\min} = \tilde{U}_q(x_{\min}, \epsilon, q)$ exists.

It is important to note that, for cases with $q > 1$ and $x_{\rm in} \ll 1$, there can be two turning points in the effective potential $\tilde{U}_q$ for the energy levels $\tilde{E} = -k_z^2 r_0^2$ ($[x_1]_{\min}$ and $[x_1]_{\max}$). It is also possible that $\tilde{E} < [\tilde{U}_q]_{\min}$, and stable negative energy levels (corresponding to MRI modes) do not exist. If the dimensionless radius of the inner disk $x_{\rm in}$ falls between the roots of the effective potential $\tilde{U}_q$, then a free boundary of the flow occurs at the point $x_{\rm in}$, as in the previously considered $q = 0$ case.

Thus, the analysis of the shape of the effective potential $\tilde{U}_q$ indicates the need to take it into account when considering global MRI in specific physical cases.

4. Summary and discussion

4.1 Nonlocal modal analysis with constant background magnetic field

We have revisited the development of MRI in Keplerian flows of an ideal fluid. We have shown that taking into account radial nonlocality in the analysis of perturbations in the form of $f(r)\exp(\mathrm{i}(\omega t - k_z z))$ leads to the appearance of the term $-(3/4)(1/r^2)$ in Eqn (17) for small perturbations. The equation for small perturbations takes the form of a stationary Schrödinger equation with an effective potential that determines (in the form of a dispersion equation) the region of negative ω^2 values — the region of MRI growth. The neutral mode $\omega^2 = 0$ corresponds to the critical magnetic field (36). The critical field in terms of the Alfvén velocity $c_{\rm A}^2$ is given by $(c_{\rm A})_{\rm cr}^2 = 4GM/r_0$, where r_0 is the zero point of the potential U (22) in Eqn (17).

The second important result is the significant reduction (compared to the local analysis) in the MRI instability increment for the case of $c_{\rm A}^2 \ll (c_{\rm A})_{\rm cr}^2$ (see Eqn (38)). Indeed, ignoring the term $-(3/4)(1/r^2)$ in equation (17) and replacing the derivative $\partial/\partial r \to -\mathrm{i}k_r$, equation (17) transforms into a fourth-degree algebraic equation with the solution

$$\omega^2 = \left(\frac{k_z}{k}\right)^2 \left[c_{\rm A}^2 k_z^2 + \frac{\Omega^2}{2} - \sqrt{\frac{\Omega^4}{4} + 4\Omega^2 c_{\rm A}^2 k^2} \right] \qquad (77)$$

(here, $k^2 = k_r^2 + k_z^2$). The maximal instability increment in this case is independent of the magnetic field strength:

$$\omega_{\max}^2 = -\frac{9}{16}\left(\frac{k_z}{k}\right)^2 \Omega^2 . \qquad (78)$$

We stress the difference between the local result (78) and the nonlocal result (39). In the nonlocal approach, a critical magnetic field that suppresses MRI appears, which was absent in the local modal analysis (see, for example, [10, 31]). In the global analysis, the maximum increment of MRI is achieved at a specific value of the Alfvén velocity, $(c_{\rm A}/(c_{\rm A})_{\rm cr})^2 = 5/16$ (see Fig. 5 and Eqn (39)). The fact that MRI arises only in sufficiently weak magnetic fields was already noted in the seminal work [10] (see also, for example, subsequent studies [32, 33], etc.). For small magnetic fields, $c_{\rm A} \ll (c_{\rm A})_{\rm cr}$, the instability increment is suppressed by a factor of $3(c_{\rm A}/(c_{\rm A})_{\rm cr})$, as shown by Eqn (38).

We emphasize that, as shown by numerical analysis (see Appendix A), in 'shallow' potential wells with the dimensionless inner radius of the flow $x_{\rm in} = r_{\rm in}/r_0 > 0.8$, there are no stationary eigenmodes (17), i.e., MRI is absent there. For $x_{\rm in} = r_{\rm in}/r_0 < 0.8$, stationary levels arise, corresponding to very small k_z and large perturbation wavelengths. The number of stationary levels increases as $x_{\rm in}$ decreases. In thin Keplerian accretion disks, perturbations with wave lengths $\lambda = 2\pi/k_z$ smaller than the disk's semi-thickness h exist only in 'deep' potential wells with $\log x_{\rm in} < -3.756$. Therefore, the standard formulation of MRI (shearing flow immersed in a constant poloidal magnetic field) does not always work in thin accretion disks. For example, in accretion disks around ordinary stars (shallow potentials), the inner disk radius may be too large for the appearance of short-wavelength unstable modes, while, in accretion disks around compact stars (deep potentials), unstable modes with wavelengths smaller than the disk thickness are possible.

4.2 Nonlocal modal analysis with a radially changing background magnetic field

We have performed, for the first time, a nonlocal modal analysis of MRI with a variable background Alfvén velocity $c_{\rm A}(r)$ and extensively studied the case of a power-law dependence $c_{\rm A}^2(r) \propto r^{-q}$ in Keplerian flows (equations for small perturbations of the magnetic field (62) and (63), respectively). We have found that the maximum growth rate of MRI increases with increasing q (Fig. 6). Furthermore, in this case, the dimensionless potential $\tilde{U}_q$ (75) depends on both q and the parameter $\epsilon = c_{\rm A}^2(r_0)/v_\phi^2(r_0)$. For $q > 1$, the potential $\tilde{U}(q, \epsilon)$ qualitatively changes with decreasing ϵ from the critical value (corresponding to the zero mode $\omega^2 = 0$, Eqn (72)): two turning points appear to the right and left of the zero point r_0 (see Figs 9–11). Clearly, the result of the nonlocal analysis of MRI will depend on the position of the inner boundary of the flow $x_{\rm in}$ relative to the zero points of the effective potential.

Thus, the nonlocal analysis of MRI demonstrates the need to consider specific features of the flow. Here, we have only considered the poloidal background magnetic field. In real situations, there may be poloidal components as well as toroidal components of the background magnetic field. A global analysis of nonaxisymmetric perturbations for MRI has been conducted, for example, in [34]. The toroidal magnetic field in the disk plane should be subject to the Parker instability [9], which arises in the presence of gravity (Fig. 12). A detailed description of the Parker instability in accretion disks can be found, for example, in [15]. The Parker instability in accretion disks can be dubbed 'magneto-gravitational instability.'

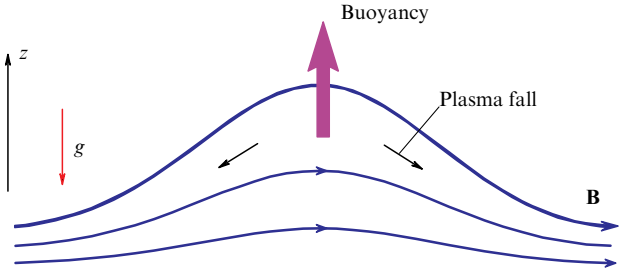

Figure 12. Schematic of the Parker instability.

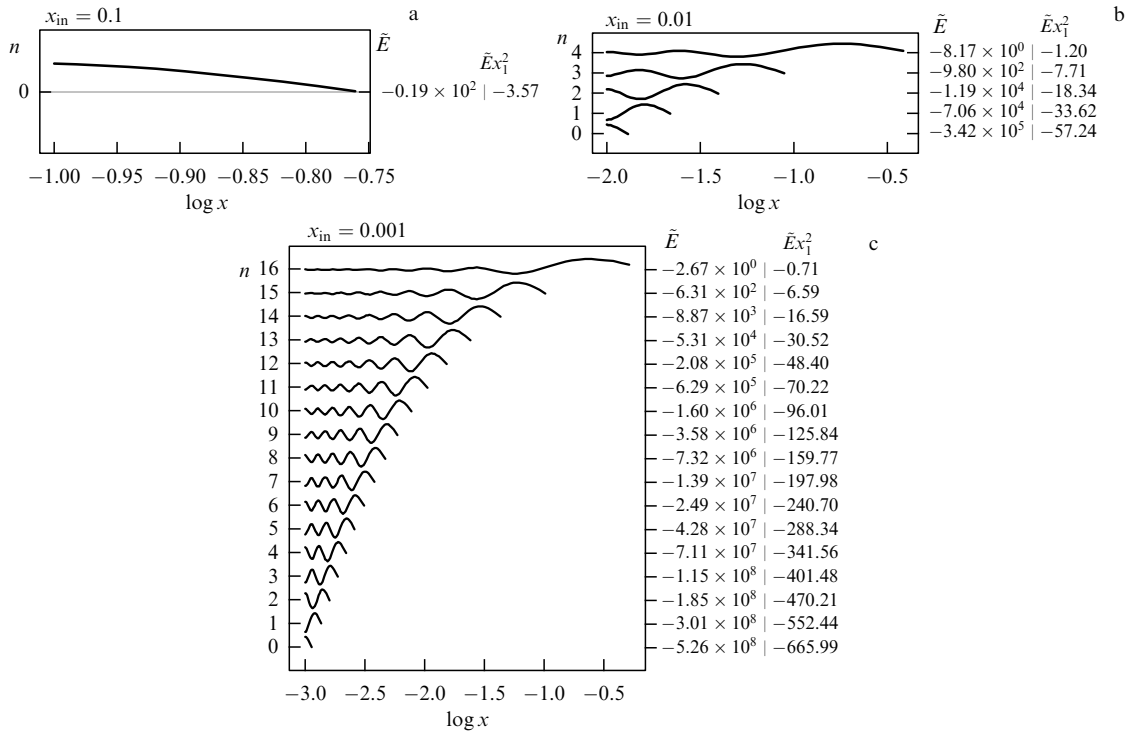

Figure 13. Normalized solutions of Eqn (79), plotted as $\Psi/\Psi_{\max}$, with boundary condition (30), $\Psi'|_{x_{in}} + \Psi/(2x_{in}) = 0$ at x_{in}, and (83) on $\Psi'(x_1)$ at x_1, corresponding to $\lim_{x\to\infty} \Psi(x) = 0$, for $x_{in} = 10^{-1}$ (a), 10^{-2} (b), and 10^{-3} (c). As x_{in} decreases (indicating a deeper potential well), the number of stationary negative energy levels increases. Exponentially decaying part of the solution for $x > x_1$ is not shown.

Acknowledgments. We express our gratitude to the reviewers for their careful reading of the article and their critical comments, which have significantly improved the presentation of the obtained results.This work was supported by the Russian Science Foundation (grant no. 21-12-00141). The authors would like to thank the participants in the seminars at the Department of Relativistic Astrophysics, Sternberg Astronomical Institute, Moscow State University, and the Theoretical Department of the Keldysh Institute of Applied Mathematics for valuable discussions.

5. Appendix

A. Numerical solution of Equation (17) for $r_{out} > r_0$

It is instructive to directly solve Eqn (17) for the case when the outer boundary of the flow lies beyond the point r_0, where the potential $U(r_0) = 0$. In dimensionless variables $x = r/r_0$ and $\tilde{E} = -k_z^2 r_0^2$, Eqn (17) reads

$$\frac{\mathrm{d}^2\Psi}{\mathrm{d}x^2} + \{\tilde{E} - \tilde{U}\}\Psi = 0\,, \quad \tilde{U} = \frac{3}{4}\frac{1}{x^2} - \frac{3}{4}\frac{1}{x^3}\,. \tag{79}$$

The amplitude of the function Ψ is arbitrary, and we choose $|\Psi(x_1)| = 1$. Conditions at the boundaries of the flow are imposed according to (30).

We can simplify the numerical solution by imposing a condition not at the outer boundary point $x_{out} > 1$ but at the turning point $x_1 < 1$. At the turning point x_1, the condition $\Psi''(x_1) = 0$ is automatically satisfied due to the nature of the turning point, where $\tilde{U}(x_1) = \tilde{E}$. Therefore, as a boundary condition at the turning point, we should take the value of the first derivative $\Psi'(x_1)$. It can be easily found by noticing that, for small $\xi = x - x_1 \ll 1$, Eqn (79) reduces to the Airy equation

$$\Psi''(z) + z\,\Psi = 0\,, \tag{80}$$

where

$$z = \left(\frac{3}{2}\frac{1}{x_1^3} - \frac{9}{4}\frac{1}{x_1^4}\right)^{1/3}\xi\,. \tag{81}$$

The general solution of Eqn (80) is

$$\Psi(z) = C_1\,\mathrm{Ai}\,(-z) + C_2\,\mathrm{Bi}\,(-z)\,. \tag{82}$$

It should be clear that, if the outer boundary $x_{out} \to \infty$, then $\Psi \to 0$, and the constant in the general solution C_2 must be equal to zero. For a finite x_{out}, the constant C_2 is nonzero, and the value of the first derivative $\Psi'(x_1)$ should be determined from the conditions at the outer and inner boundaries (30). Below, we present solutions for the case of $x_{out} \gg 1$ with the constant $C_2 = 0$.

At the point x_1, where $\xi = z = 0$, the first derivative reads

$$\left.\frac{\mathrm{d}\Psi}{\mathrm{d}x}\right|_{x_1} = \left.\frac{\mathrm{d}\Psi}{\mathrm{d}z}\frac{\mathrm{d}z}{\mathrm{d}x}\right|_{x_1} = C_1\,\mathrm{Ai}'(0)\left[\frac{3}{2}\frac{1}{x_1^3} - \frac{9}{4}\frac{1}{x_1^4}\right]^{1/3}, \tag{83}$$

where $\mathrm{Ai}'(0) = 0.25882\ldots$.

Integrating Eqn (79) with the boundary conditions (30) $\Psi'|_{x_{in}} + \Psi/(2x_{in}) = 0$ and Eqn (83) for various values of x_{in} yields a family of solutions with discrete (nonequidistant) 'energy levels' $\tilde{E}_n$ (or, equivalently, according to Eqn (27), with discrete turning points x_1) corresponding to the integer number $n = 0, 1, 2, 3, \ldots$ of the zeros of the function Ψ. It should be noted that, for a given x_{in}, a different number of possible energy levels exists, and there is a maximum value $(x_{in})_{\max} \approx 0.8116$ that allows the existence of a single level for $n = 0$. The solutions, normalized to the maximum value of the

function Ψ, are shown in Fig. 13. The discrete 'energy levels' $\tilde{E} = -(k_z r_0)^2$ of Eqn (79) for different inner boundaries $x_{\rm in}$ are shown in Fig. 14. The values of the energy $\tilde{E}$ for different levels at fixed $x_{\rm in}$ under various boundary conditions on the function Ψ are presented in Table 1. It is evident that the type of boundary conditions has a weak influence on the energy values of the 'lower' levels in deep potential wells for $x_{\rm in} \ll 1$.

It should be noted that Eqn (79) can be solved using the quasiclassical (WKB) approximation, employing the Bohr–Sommerfeld condition for discrete energy levels $E = -k_z^2 < 0$ with index $n = 0, 1, 2, \ldots$ in the potential U for rigid boundaries [27, 28]:

$$\int_{r_{\rm in}}^{r_1} \sqrt{E - U}\, {\rm d}r = \pi\left(n + \frac{3}{4}\right); \quad n = 0, 1, 2, \ldots . \tag{84}$$

Here, r_1 is the turning point in the potential U, which can be found from Eqn (26). The existence of stationary levels with negative energy and $\omega^2 < 0$ indicates the instability of the flow. A similar equation, but with a constant slightly different from 3/4, can be obtained for a free boundary. However, for large $n \gg 1$, all three boundary conditions ($\Psi|_{x_{\rm in}} = 0$, $\Psi'|_{x_{\rm in}} = 0$, $(\Psi' + \Psi/(2x))|_{x_{\rm in}} = 0$) yield the same result.

In dimensionless units with energy $\tilde{E} = -k_z^2 r_0^2$ and potential $\tilde{U}$, Eqn (84) takes the form

$$\int_{x_{\rm in}}^{x_1} \sqrt{\tilde{E} - \frac{3}{4x^2} + \frac{3}{4x^3}}\, {\rm d}x = \pi\left(n + \frac{3}{4}\right). \tag{85}$$

In the case of a large perturbation wavelength, $\tilde{E} = -k_z^2 r_0^2 \ll 1$. At low energies $\tilde{E} \approx 0$, the turning point tends to the zero of the potential, $r_1 \to r_0$, and the integral in Eqn (85) is

$$\int_{x_{\rm in}}^{1} \sqrt{-\frac{3}{4x^2} + \frac{3}{4x^3}}\, {\rm d}x = \pi\left(n + \frac{3}{4}\right). \tag{86}$$

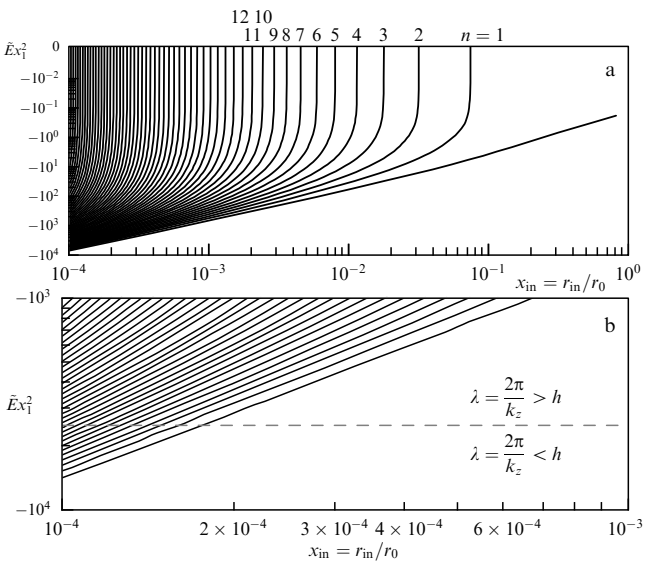

Figure 14. (a) Discrete 'energy levels' $\tilde{E} = -(k_z r_0)^2$ of Eqn (79) for different inner boundaries $x_{\rm in}$. As $x_{\rm in}$ decreases, number of discrete 'energy levels' $n = 0, 1, 2, 3, \ldots$ of function Ψ increases. Deep 'energy levels' with $-\tilde{E}x_1^2 > 4 \times 10^3$ appear when $\log x_{\rm in} < -3.756$. A maximum value of $x_{\rm in} \approx 0.8116$ with $\tilde{E}_0 \approx -0.2644$ exists for the eigenmode with $n = 0$. Other modes $n = 1, 2, \ldots$ can have $\tilde{E} = 0$ at certain values of $x_{\rm in}$. (b) Region of 'deep levels' and boundary $\lambda = 2\pi/k_z = h = 0.1r$ for thin accretion discs (see Section 2.6).

This integral is taken as follows:

$$\sqrt{3}\left[\sqrt{\frac{1}{x_{\rm in}} - 1} + \arcsin\sqrt{x_{\rm in}} - \frac{\pi}{2}\right] = \pi\left(n + \frac{3}{4}\right) \tag{87}$$

(compare with equation (2.24) for the case of isomoment rotation with circular velocity $v_\phi \propto 1/r$ in the original paper by [6]; here, we consider the Keplerian case with $v_\phi \propto 1/\sqrt{r}$). From Eqn (87), we find the first $x_{\rm in}$ for $n = 0$: $x_{\rm in} \approx 0.575$. The exact value, which we obtained numerically (see Fig. 14), is $(x_{\rm in})_{\max} \approx 0.8116$. Furthermore, under the given third-type boundary conditions, the energy value for the mode with $n = 0$ is approximately $\tilde{E}[(x_{\rm in})_{\max}] \approx -0.2644$, and for modes $n = 1, 2, \ldots$, there is always a discrete value of $x_{\rm in}$ for which $\tilde{E} = 0$. For first- and second-type boundary conditions, $E[(x_{\rm in})_{\max}] = 0$ (see Table 1 and 2 for different conditions at the inner boundary). For $x_{\rm in} > (x_{\rm in})_{\max}$, the potential well becomes so shallow that there are no stationary 'energy levels.' It is worth noting that the accuracy of the WKB approximation increases for large n. In our case, for $x_{\rm in} = r_{\rm in}/r_0 \ll 1$, the discrete values of $x_{\rm in}$ are given by

$$x_{\rm in} = \frac{1}{\left[(\pi/\sqrt{3})(n + 3/4) + \pi/2\right]^2 + 1}\,. \tag{88}$$

In principle, the integral in Eqn (85) can be numerically computed for any value of $\tilde{E}$ to find the discrete energy levels $\tilde{E}_n$ at fixed $x_{\rm in}$ (especially for large $|\tilde{E}|$ corresponding to thin accretion disks, as mentioned above) for any n. However, precise numerical solutions of Eqn (79) have already been obtained.

It is worth noting that, if we disregard the term $3/(4x^2)$ in Eqn (85), it can be solved analytically (see [22]). The WKB

Table 1. Examples of energy levels $\tilde{E}$ of Eqn (79) for $x_{\rm in} = 0.1, 0.01, 0.001$ and different conditions at the inner boundary $x_{\rm in}$.

$n_{\tilde{E}}$	$(\Psi' + \Psi/(2x))\|_{x_{\rm in}} = 0$	$\Psi'\|_{x_{\rm in}} = 0$	$\Psi\|_{x_{\rm in}} = 0$
$x_{\rm in} = 0.1$			
0	-118.86	-86.44	—
$x_{\rm in} = 0.01$			
4	-8.168	-7.096	—
3	-9.799×10^2	-9.250×10^2	-1.229×10^2
2	-1.189×10^4	-1.145×10^4	-3.483×10^3
1	-7.057×10^4	-6.846×10^4	-2.808×10^4
0	-3.423×10^5	-3.288×10^5	-1.408×10^5
$x_{\rm in} = 0.001$			
16	-2.666	-2.525	—
15	-6.314×10^2	-6.190×10^2	-7.436×10^1
14	-8.869×10^3	-8.762×10^3	-2.668×10^3
13	-5.308×10^4	-5.260×10^4	-2.266×10^4
12	-2.078×10^5	-2.063×10^5	-1.071×10^5
11	-6.287×10^5	-6.250×10^5	-3.650×10^5
10	-1.598×10^6	-1.590×10^6	-1.007×10^6
9	-3.585×10^6	-3.569×10^6	-2.397×10^6
8	-7.319×10^6	-7.290×10^6	-5.121×10^6
7	-1.390×10^7	-1.385×10^7	-1.007×10^7
6	-2.495×10^7	-2.486×10^7	-1.857×10^7
5	-4.284×10^7	-4.271×10^7	-3.258×10^7
4	-7.115×10^7	-7.094×10^7	-5.496×10^7
3	-1.155×10^8	-1.151×10^8	-9.011×10^7
2	-1.854×10^8	-1.848×10^8	-1.451×10^8
1	-3.005×10^8	-2.994×10^8	-2.328×10^8
0	-5.263×10^8	-5.227×10^8	-3.828×10^8

Table 2. Values of the dimensionless inner flow boundary for zero energy $x_{\rm in}|_{\tilde{E}=0}$ under different choices of boundary conditions. Value of $x_{\rm in}|_{\tilde{E}=0}$ in the WKB approximation is given by (87) and (88). It is noteworthy that under the third-type boundary condition (free boundary) the zero energy level is reached at a finite value of $\tilde{E} \approx -0.2644$ corresponding to $x_{\rm in} \approx 0.8116$. Refer to Fig. 14 for further details.

$n_{\tilde{E}}$	$(\Psi' + \Psi/(2x))\|_{x_{\rm in}} = 0$	$\Psi'\|_{x_{\rm in}} = 0$	$\Psi\|_{x_{\rm in}} = 0$
...	...	...	...
16	1.02496×10^{-3}	1.02426×10^{-3}	—
15	1.15546×10^{-3}	1.15457×10^{-3}	1.08531×10^{-3}
14	1.31260×10^{-3}	1.31145×10^{-3}	1.22775×10^{-3}
13	1.50417×10^{-3}	1.50266×10^{-3}	1.40021×10^{-3}
12	1.74105×10^{-3}	1.73903×10^{-3}	1.61176×10^{-3}
11	2.03875×10^{-3}	2.03598×10^{-3}	1.87519×10^{-3}
10	2.42010×10^{-3}	2.41620×10^{-3}	2.20897×10^{-3}
9	2.91976×10^{-3}	2.91407×10^{-3}	2.64061×10^{-3}
8	3.59244×10^{-3}	3.58384×10^{-3}	3.21255×10^{-3}
7	4.52880×10^{-3}	4.51513×10^{-3}	3.99300×10^{-3}
6	5.88807×10^{-3}	5.86497×10^{-3}	5.09744×10^{-3}
5	7.97202×10^{-3}	7.92969×10^{-3}	6.73423×10^{-3}
4	1.14131×10^{-2}	1.13263×10^{-2}	9.31161×10^{-3}
3	1.77392×10^{-2}	1.75298×10^{-2}	1.37231×10^{-2}
2	3.15576×10^{-2}	3.08961×10^{-2}	2.22593×10^{-2}
1	7.39693×10^{-2}	7.03546×10^{-2}	4.24509×10^{-2}
0	$0.8116\|_{\tilde{E}=-0.2644}$	5.87626×10^{-1}	1.14244×10^{-1}

solution is found to be in excellent agreement with the numerical results.

B. For $r_{\rm out} < r_0$

If the outer boundary of the flow, denoted as $r_{\rm out}$, is smaller than r_0 (the point at which the potential becomes zero, $U(r_0) = 0$, see Eqn (23)), then the problem of finding the stationary energy levels of Eqn (79) needs to be numerically solved with the boundary conditions given by (30). In the case of a narrow flow (when the outer radius is close to the inner radius), the problem has an analytical solution. A similar problem, with a different rotational law and zero boundary conditions for magnetic field perturbations ($b_r = 0$, corresponding to the condition $\Psi = 0$), was solved by [6]. Let us introduce the following notations:

$$\bar{r} \equiv r_{\rm in} + \frac{r_{\rm out} - r_{\rm in}}{2}\,, \qquad \Delta \equiv r_{\rm out} - r_{\rm in} \ll \bar{r}\,. \tag{89}$$

When the parameter $\bar{r}$ is fixed, Eqn (79) transforms into a Sturm–Liouville problem with homogeneous boundary conditions of the third kind in the interval $x \in [a, b]$:

$$\begin{cases} \Psi'' + \lambda\Psi = 0\,, \\ \Psi'|_a + \dfrac{\Psi}{2a} = 0\,, \\ \Psi'|_b + \dfrac{\Psi}{2b} = 0\,, \end{cases} \tag{90}$$

where

$$\lambda = -k_z^2 - \frac{3}{4}\frac{1}{\bar{r}^2} + \frac{GM}{\bar{r}^3}\,\frac{\omega^2/k_z^2 + 3c_{\rm A}^2}{\left(c_{\rm A}^2 - \omega^2/k_z^2\right)^2}\,. \tag{91}$$

This problem allows the existence of only positive nontrivial eigenvalues $\lambda_n > 0$, corresponding to oscillating eigenfunctions Ψ_n. Then, the general solution of Eqn (90) is given by

$$\Psi = C_1 \sin\left(\sqrt{\lambda}x\right) + C_2 \cos\left(\sqrt{\lambda}x\right). \tag{92}$$

The constants C_1 and C_2 are determined by the boundary conditions. By excluding the trivial solution $\lambda = 0$, we obtain the following system of equations:

$$\begin{cases} C_1\left(1 + \dfrac{1}{2\sqrt{\lambda}a}\tan\left(\sqrt{\lambda}a\right)\right) + C_2\left(\dfrac{1}{2\sqrt{\lambda}a} - \tan\left(\sqrt{\lambda}a\right)\right) = 0\,, \\ C_1\left(1 + \dfrac{1}{2\sqrt{\lambda}b}\tan\left(\sqrt{\lambda}b\right)\right) + C_2\left(\dfrac{1}{2\sqrt{\lambda}b} - \tan\left(\sqrt{\lambda}b\right)\right) = 0\,. \end{cases} \tag{93}$$

System (93) has a nontrivial solution when the determinant is equal to zero. This leads to a transcendental equation for finding the eigenvalues λ:

$$\left[\frac{1}{2\sqrt{\lambda}b} - \frac{1}{2\sqrt{\lambda}a}\right]\left(1 + \tan\left(\sqrt{\lambda}a\right)\tan\left(\sqrt{\lambda}b\right)\right) + \left[1 + \frac{1}{4\lambda ab}\right]\left(\tan\left(\sqrt{\lambda}a\right) - \tan\left(\sqrt{\lambda}b\right)\right) = 0\,. \tag{94}$$

Equation (94) has two families of solutions:

$$\begin{cases} 1 + \tan\left(\sqrt{\lambda}a\right)\tan\left(\sqrt{\lambda}b\right) = 0\,, \\ -\tan\left(\sqrt{\lambda}(b-a)\right) = \dfrac{\sqrt{\lambda}(b-a)}{1 + 4\lambda ab}\,. \end{cases} \tag{95}$$

The first family of solutions to Eqn (94) is given by

$$\cos\left(\sqrt{\lambda}\,[a-b]\right) = 0\,. \tag{96}$$

From this, we obtain the set of eigenvalues

$$\lambda_n = \frac{\left(\pi/2 + n\pi\right)^2}{\Delta^2}\,, \qquad n = 0, 1, 2, 3, \ldots\,. \tag{97}$$

For small values of $n = 1, 2, 3, \ldots$, the second family of solutions (95) can be found numerically. However, for large argument values, it quickly converges to $\lambda_n \approx \pi^2 n^2/\Delta^2$ for $n \gg 1$. Therefore, for large n, both solutions can be combined into a single expression: $\lambda_n \approx (\pi^2/4)(1+n)^2/\Delta^2$. It should be noted that, under first-kind homogeneous boundary conditions $\Psi|_{a,b} = 0$ or second-kind homogeneous boundary conditions $\Psi'|_{a,b} = 0$, the following solutions are obtained:

$$\begin{aligned} &\sin\sqrt{\lambda}\,(b-a) = 0 \rightarrow \lambda_n = \frac{\pi^2 n^2}{\Delta^2}\,, \\ &\sin\sqrt{\lambda}\,(a+b) = 0 \rightarrow \lambda_n = \frac{\pi^2 n^2}{(a+b)^2}\,, \\ &n = 1, 2, 3, \ldots\,. \end{aligned} \tag{98}$$

From (97), we obtain a set of equations for each eigenvalue λ_n:

$$-k_z^2 - \frac{3}{4}\frac{1}{\bar{r}^2} + \frac{GM}{\bar{r}^3}\,\frac{\omega^2/k_z^2 + 3c_{\rm A}^2}{\left(c_{\rm A}^2 - \omega^2/k_z^2\right)^2} = \lambda_n \approx \frac{\pi^2(n+1)^2}{4\Delta^2}\,, \quad n = 0, 1, 2, 3, \ldots\,. \tag{99}$$

Hence, we obtain the dispersion equations in the following form:

$$\begin{aligned} &\frac{\omega^2}{c_{\rm A}^2 k_z^2} = \left(1 + \frac{K}{2}\right)\left[1 \pm \sqrt{1 + \frac{4(3K-1)}{(K+2)^2}}\,\right], \\ &K \approx \left(\frac{v_\phi^2(\bar{r})}{c_{\rm A}^2}\right)\frac{1}{(\pi^2/4)(n+1)^2\left(\bar{r}/\Delta\right)^2 + k_z^2\,\bar{r}^2 + 3/4}\,. \end{aligned} \tag{100}$$

For unstable modes with $\omega^2 < 0$, in the dispersion equation (100), we keep the minus sign before the square root and require $K > 1/3$, which leads to the appearance of a critical

magnetic field for the MRI mode:

$$c_{\rm A}^2 < (c_{\rm A}^2)_{\rm cr} \approx \frac{4v_\phi^2(\bar{r})}{(1/3)\,\pi^2(n+1)^2(\bar{r}/\Delta)^2 + (4/3)\,k_z^2\,\bar{r}^2 + 1}\,. \tag{101}$$

It should be noted that, for the first- and second-kind boundary conditions, the critical field values are given by

$$\begin{cases} (c_{\rm A}^2)_{\rm cr} = \dfrac{4v_\phi^2\,(\bar{r})}{(4/3)\,\pi^2 n^2\,(\bar{r}/\Delta)^2 + (4/3)\,k_z^2\,\bar{r}^2 + 1}\,, & \Psi|_{a,b} = 0\,, \\ (c_{\rm A}^2)_{\rm cr} = \dfrac{4v_\phi^2(\bar{r})}{(1/3)\,\pi^2 n^2 + (4/3)\,k_z^2\,\bar{r}^2 + 1}\,, & \Psi'|_{a,b} = 0\,. \end{cases} \tag{102}$$

The similarity of results between the first- and third-kind boundary conditions is notable.

Lastly, it is noteworthy that, for $r_{\rm out} < r_0$ (when the potential has the same sign over the entire interval $[r_{\rm in}, r_{\rm out}]$), the asymptotic behavior of eigenvalues is given by $\lambda_n \sim \pi^2 n^2/(r_{\rm out} - r_{\rm in})^2$ for large $n \gg 1$, which follows from the general theorems of the Sturm–Liouville problem for any continuous potential with a consistent sign (see, for example, [35]).

References

1. Shakura N I, Sunyaev R A *Astron. Astrophys.* **24** 337 (1973)
2. Bisnovatyi-Kogan G S, Lovelace R V E *New Astron. Rev.* **45** 663 (2001)
3. Lipunova G, Malanchev K, Shakura N, in *Accretion Flows in Astrophysics* (Astrophysics and Space Science Library, Vol. 454, Ed. N Shakura) (Cham: Springer, 2018) p. 1, https://doi.org/10.1007/978-3-319-93009-1_1
4. Boneva D V et al. *Astron. Astrophys.* **652** A38 (2021)
5. Somov B V et al. *Adv. Space Res.* **32** 1087 (2003)
6. Velikhov E P *Sov. Phys. JETP* **9** 995 (1959); *Zh. Eksp. Teor. Fiz.* **36** 1398 (1959)
7. Chandrasekhar S *Proc. Natl. Acad. Sci. USA* **46** 253 (1960)
8. Strutt J W (Lord Rayleigh) *Proc. R. Soc. Lond. A* **93** 148 (1917)
9. Parker E N *Astrophys. J.* **145** 811 (1966)
10. Balbus S A, Hawley J F *Astrophys. J.* **376** 214 (1991)
11. Balbus S A, Hawley J F *Rev. Mod. Phys.* **70** 1 (1998)
12. Hawley J F, Gammie C F, Balbus S A *Astrophys. J.* **440** 742 (1995)
13. Sorathia K A et al. *Astrophys. J.* **749** 189 (2012)
14. Hawley J F et al. *Astrophys. J.* **772** 102 (2013)
15. Kato S, Fukue J, Mineshige S *Black-Hole Accretion Disks* (Kyoto, Japan: Kyoto Univ. Press, 1998)
16. Shakura N, Postnov K *Mon. Not. R. Astron. Soc.* **451** 3995 (2015)
17. Zou R et al. *Phys. Rev. E* **101** 013201 (2020)
18. Papaloizou J, Szuszkiewicz E *Geophys. Astrophys. Fluid Dyn.* **66** 223 (1992)
19. Kumar S, Coleman C S, Kley W *Mon. Not. R. Astron. Soc.* **266** 379 (1994)
20. Gammie C F, Balbus S A *Mon. Not. R. Astron. Soc.* **270** 138 (1994)
21. Curry C, Pudritz R E, Sutherland P G *Astrophys. J.* **434** 206 (1994)
22. Latter H N, Fromang S, Faure J *Mon. Not. R. Astron. Soc.* **453** 3257 (2015)
23. Knobloch E *Mon. Not. R. Astron. Soc.* **255** 25P (1992)
24. Dubrulle B, Knobloch E *Astron. Astrophys.* **274** 667 (1993)
25. Shakura N I, Lipunova G V *Mon. Not. R. Astron. Soc.* **480** 4273 (2018)
26. Shakura N, Postnov K *Mon. Not. R. Astron. Soc.* **448** 3697 (2015)
27. Landau L D, Lifshitz E M *Quantum Mechanics. Non-Relativistic Theory* (Oxford: Butterworth-Heinemann, 1998); Translated from Russian: *Kvantovaya Mekhanika. Nerelyativistskaya Teoriya* (Moscow: Nauka, 1989)
28. Flügge S *Practical Quantum Mechanics* (Berlin: Springer-Verlag, 1971) in 2 Vols
29. Landau L D, Lifshitz E M *Fluid Dynamics* (Oxford: Pergamon Press, 1987); Translated from Russian: *Gidrodinamika* (Moscow: Nauka, 1986)
30. Acheson D J *Elementary Fluid Dynamics* (Oxford: Clarendon Press, 1990)
31. Shakura N, Postnov K, in *Accretion Flows in Astrophysics* (Astrophysics and Space Science Library, Vol. 454, Ed. N Shakura) (Cham: Springer, 2018) p. 393, https://doi.org/10.1007/978-3-319-93009-1_8
32. Salmeron R, Königl A, Wardle M *Mon. Not. R. Astron. Soc.* **375** 177 (2007)
33. Bai X-N, Stone J M *Astrophys. J.* **769** 76 (2013)
34. Curry C, Pudritz R E *Mon. Not. R. Astron. Soc.* **281** 119 (1996)
35. Levitan B M, Sargsyan I S *Operatory Shturma–Liuvillya i Diraka* (Sturm – Liouville and Dirac Operators) (Moscow: Nauka, 1988)